APPLICATIONS OF MACHINE LEARNING FOR PIPELINE INTEGRITY MANAGEMENT SYSTEMS

A Thesis

by

ADITHYAA KARTHIKEYAN

Submitted to the Office of Graduate and Professional Studies of
Texas A&M University
in partial fulfillment of the requirements for the degree of

MASTER OF SCIENCE

Chair of Committee:	Byul Hur
Co-Chair of Committee:	Saadat Mirza
Committee Members:	William Ronald Ledbetter
	Gregory Pearlstein
Head of Department:	Timothy Jacobs

May 2020

Major Subject: Interdisciplinary Engineering

ABSTRACT

Oil and gas pipelines that traverse a river are often buried beneath the river bed and channel banks. One of the primary reasons for the exposure of buried pipelines is the scouring mechanism that occurs when the shear stress induced on riverbed by flowing water exceeds the resistance of channel bed material. Depending on the free spanning length and watercourse flow velocity, the vortex shedding phenomena may cause interactions resulting in a catastrophic pipeline failure and disrupting the integrity of the pipeline system. Hence it is essential to accurately predict Critical Span Length (CSL) and scour depth for river crossing pipelines.

Estimates of CSL and scour depth are found in literature subject to various governing factors. It is difficult to model the physics of the free span scenario considering all parameters associated with the pipeline. Advances in soft computing techniques has opened a whole new dimension to predict design parameters that are difficult to mathematically model, thus enabling protective preparations to maintain integrity and prevent failures.

In this study, we attempt to identify measurable factors to predict CSL and scour depth and understand the effect of these variables using Artificial Neural Networks. An Artificial Neural Network model is developed by collecting pipeline accident reports from Pipeline and Hazardous Materials Safety Administration (PHMSA) database for accidents that occurred due to Vortex Induced Vibration (VIV) loading during flooding in the last 35 years. This is done by identifying parameters that describe the pipeline including but not limited to pipe dimensions, pipe material properties, exposure flow rate, river velocity and dynamic lateral and vertical soil stiffness from real time data. The neural network model designed in MATLAB quickly and accurately predicts critical span length and scour depth for several river crossing pipelines and the results are compared to Finite Element Analysis and numerical simulations. This model can help us assess which flooding conditions would potentially cause a VIV failure in the pipe, once exposure flow rates and river velocities are estimated.

ACKNOWLEDGMENTS

I would like to express my sincere gratitude to my advisors, Dr. Byul Hur and Dr. Saadat Mirza, for their invaluable support and guidance throughout this research. Also, I am grateful for their precious time and constructive suggestions on this research work.

I am thankful to all of my committee members, Prof. William Ronald Ledbetter and Dr. Gregory Pearlstein for their valuable insights and comments that helped me in finding the right direction on this research.

I take this opportunity to convey my special thanks to Mr. Aravind Nair, Deputy Head of Section, DNV GL for helping me with the problem formulation during the initial phase of this research work.

I would like to express my heartfelt gratitude to Dr. Timothy Jacobs and Prof. Julie Ingram for being a pillar of support and strength throughout this program in Texas A&M University.

I would like to show my special thanks to Ms. Rachal Thomassie and Ms. Kim Moses for their constant support during my study here in Texas A&M University.

I am truly thankful to my parents for their unconditional trust and support in my pursuit of this research work. Finally, I would like to thank Akash, Amrita, Karthik, Ramanathan, Niranjan, Anand and Sushmitha for their friendship and the insights on Machine Learning algorithms and their applications.

CONTRIBUTORS AND FUNDING SOURCES

Contributors

This work was supervised by a dissertation committee consisting of Dr. Byul Hur [Chair] from the Department of Engineering Technology and Industrial Distribution (ETID), Dr. Saadat Mirza [Co-chair] and Prof. William Ronald Ledbetter from the Department of Interdisciplinary Engineering and Dr. Gregory Pearlstein from the Department of Mathematics. Professor Saadat Mirza's guidance was invaluable in collecting data for relevant input features from various sources.

Funding Sources

All work for the dissertation was completed independently by the student. There is no outside funding contributions to acknowledge related to the research and compilation of this document.

NOMENCLATURE

ANN	Artificial Neural Networks
CSL	Critical Span Length, (also) Maximum Allowable Free Span Length
DNV	Det Norske Veritas
FSR	Free Span Ratio
IoT	Internet of Things
LM	Levenberg-Marqaurdt Training algorithm
MAFSL	Maximum Allowable Free Span Length, (also) Critical Span Length
MARS	Multivariate Adaptive Regression Splines
MSE	Mean Square Error
NOAA	National Oceanic and Atmospheric Administration
NPMS	National Pipeline Mapping System
PHMSA	Pipeline and Hazardous Materials Safety Administration
USGS	United States Geological Survey
VIV	Vortex Induced Vibrations

TABLE OF CONTENTS

Page

LIST OF FIGURES

FIGURE Page

LIST OF TABLES

TABLE Page

1. INTRODUCTION

Pipeline integrity management is one of the most extensively carried out programs across the world that focuses on the safety aspects and environmental risks associated with hazardous liquid and natural gas pipelines. It is the cradle-to-grave approach of understanding and operating pipelines in a safe, reliable manner. Pipelines have been used to transport large quantities of energy products across the country for decades. However, they present substantial threat of low probability, high consequence accidents that result in environmental degradation and human casualties in certain cases. With the recent advancement in computational intelligence, in the area of machine learning in particular, the possibility of a very low pipeline failure has come close to reality than ever before.

Converting volumes of raw data from different engineering disciplines into useful information is a challenge for Oil and Gas companies. One of the fundamental focal points in data driven modeling approach is to discover relationships between the system input and output state variables without explicit knowledge of the physical behavior of the system. Increased precision and confidence in data makes a difference in operational effectiveness, efficiency, and enhanced threat detection.

Free-span management of pipelines transporting liquid and natural gas starts from the early project phases including pre-engineering survey, design and construction, and continues throughout the whole operating life. The design phase is the core of free span integrity management. Hence determination of maximum allowable free span length (MAFSL) plays a crucial role in the design of pipelines and in trouble shooting existing pipelines in river crossings. In addition, an accurate measure of scour depth potentially identifies a feasible Depth of Cover (DoC) for the pipelines to be buried during the initial laying phase.

Significant contributions are made to estimate MAFSL of pipelines in river crossings subject to different conditions and are elaborated in the literature review. It has been shown that different loading conditions lead to the exposure and failure of pipelines in different situations. There is

no single approach that entirely captures the physics of the problem. Hence, difficulties exist in the mathematical modeling of scenario considering all physical and environmental parameters associated with pipelines using the traditional deterministic approach. Artificial Neural Networks play a key role in mathematical modelling of such a system.

In the United States, pipeline operators are required to abide by regulations put forth by the federal Pipeline and Hazardous Materials Safety Administration (PHMSA), at a minimum. With a large number of historical data available from PHMSA database, the United States Geographical Survey (USGS) and the National Oceanic and Atmospheric Administration (NOAA), we have attempted to select relevant input factors to predict Critical Span Length (CSL) and Scour Depth for river crossing pipelines. The prediction model is set up using Artificial Neural Networks (ANN) to understand the non-linear variation of these factors.

2. BACKGROUND

2.1 Literature Review

Transmission pipeline infrastructure in the United States can be estimated to have more than 100,000 pipeline crossings within rivers, streams, lakes, or flood plains. Although accidents at river crossings account for less than one percent of the total number of pipeline accidents, the environmental consequence of a release in water can be severe. The impact of these spills on the environment has been analysed in terms of cost, rate of contamination of soil, average volume of release, annual ratio of water type contamination, and effects on fish, birds and terrestrial wildlife between 2010 and 2017 based on the information from the Pipeline and Hazardous Material Safety Administration (PHMSA) database by Chiara Belvederesi, Megan S. Thompson and Petr E. Komers [9]. The study was aimed at developing a regression analysis method to understand the relationship between released volume and the total elapsed time between the accident and initiation of remediation. While hazardous liquid releases on land are more easily contained, river currents can carry hazardous liquids further downstream, and it can potentially impact larger geographical areas and more communities.

Among the many different failure modes of pipeline in river crossings, the most documented pipeline failures have been caused by Vortex Induced Vibration (VIV) loading due to the exposure of unsupported free spanning pipelines to flowing water [10]. The study focused on developing a flood monitoring program to quantify threshold flood levels that would result in exposure and failure of pipeline water crossings. The flood monitoring program is in turn aimed at establishing an action plan based on the assessment of the flood scenario to reduce the consequences of a pipeline watercourse crossing failure. Prediction of fatigue life-cycles of onshore pipelines that become exposed at river crossings due to riverbed erosion was carried out using DNV GL's FATFREE software based on S-N curves approach [11]. The methodology was later converted into a screening tool to assess free span exposure and characteristics of river crossing pipelines in Canada with a

high potential for fatigue failure due to Vortex Induced Vibrations.

Many literature studies showed the assessment and modeling of VIV loading for free spanning pipelines to estimate Maximum Allowable Free Span Length (MAFSL) for both offshore and onshore water crossing pipelines [12] [13]. Rhett Dotson and Lawrence Matta discussed the analytical assessments for MAFSL by having total longitudinal stresses below the elastic code limits. They also carried out finite element assessment based on elastic and elastic-plastic modeling of pipelines for three different scenarios [14]. The influence of soil characteristics on pipeline supports in free span was analysed in determining the natural frequency of pipeline vibrations [15]. Recommendations and guidelines have been prescribed by DNV [7] to evaluate the dynamic response of a free spanning pipeline based on pipe-soil interactions [16]. Determining the combination of loads that act on the pipeline is crucial for modeling and analysis of MAFSL. Variation in factors such as line geometry or end restraints can greatly affect the nature of results. These results are based on deterministic approach.

The oil and gas industry has vast amounts of data captured by instruments and generated by simulations. We are in a period ideally positioned to combine traditional methodologies with computational intelligence characterized by data driven models. With the availability of real time geometrical survey data, the implementation of Artificial Neural Networks (ANN) to model non linear functions with several variables is increasingly finding its advantages in the industry. Performance of Multivariate Adaptive Regression Splines (MARS) was compared with Multilayer Perceptron Neural Network model in the prediction of scour depth beneath pipelines based on data available in literature by Amir Hamzeh Haghiabi [1]. The MARS model was found to have high precision for modeling scour depth and gave clear information regarding internal processes carried out in the model development due to its linear nature. However the model had less accuracy in prediction when compared to the Neural Network model. In relation to the above article, Reza Barati developed new models for scour depth estimation using regression optimization based on power functions [17]. Failure prediction of underground pipeline in non-uniform soil settlement was modeled using artificial neural networks with axial stress as the output vector and buried depth,

wall thickness, pipe diameter, precipitation level, soil modulus of elasticity, and soil density as six input vectors [18]. The development of various training algorithms and activation functions, which can be applied to the neurons has given a new dimension to Artificial Neural Network architectures to better suit our model requirements based on the nature of data available.

2.2 River bed Scour

Scouring action of river bed refers to the removal of top sediment layer and occurs when the hydraulic shear stress on the stream bed exceeds the capability of the bed material to resist motion. Scouring is a common type of erosion that exposes a buried pipeline at its approach to a crossing and could potentially impact the integrity of the pipeline due to hydrodynamic loading, fatigue caused by vortex shedding, and impact loads. Major hazards at river crossings that may expose a pipeline due to natural or environmental changes are listed below [19]:

S.No	Hazard category	Sub Hazard type
1	Episodic exposure	Local scour and river bed degradation causing vertical channel movements
2	Progressive erosion	Bank erosion, encroachment and gullying causing lateral channel movements
3	Channel Avulsion	Meandering river, debris jams, sediment accumulation and extreme flooding resulting in the development of a new conveyance route

Table 2.1: Classification of river bed erosion phenomenon.

Flow properties such as river depth, velocity and water density, river bed and soil characteristics namely dynamic lateral and vertical stiffness of soil, longitudinal slope of the river bed, size of sediment particles, initial gap between pipeline and undisturbed bed (e), and pipeline geometry including diameter and wall thickness influence localized scour below pipelines as indicated in Figure 2.1. Many studies have been conducted to understand the correlation between scour depth

below pipelines and non dimensional numbers such as Froude number (F), Reynold's number (R_e) and Shield's parameter (τ^*).

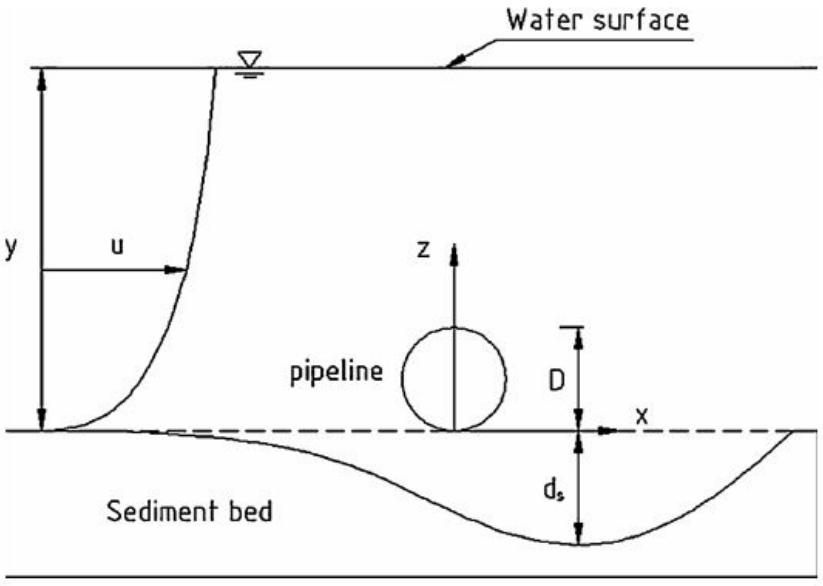

Figure 2.1: Localized scouring phenomenon below river crossing pipelines.
Note. Reprinted from [1]

Here we restrict our study on exposed pipelines due to the onset of scour in riverbeds that experience vortex induced vibrations due to the flowing water. Moncada and Aguirre-Pe (1999) presented the following relationship for estimating localized scour depth under pipelines [20],

$$\frac{d_s}{D} = 0.9 * \tanh(1.4F) + 0.55 \tag{2.1}$$

where d_s is the scour depth, F = $\frac{V}{\sqrt{gy}}$ is the Froude number, V is the velocity of river, y is the water depth and D is the pipeline outer diameter. They have also stated that parameters such as river bed slope and $\frac{e}{D}$ ratio have very minimal effect on scour depth and have been neglected in our prediction model.

2.3 Vortex Induced Vibrations: In-line and Cross-flow oscillations

Interactions between pipeline and external fluid flow (in this case, river water) which is perpendicular to the axis of the pipeline reduces the flow around the pipe and in turn induces oscillations due to the formation of vortices. This unsteady phenomenon occurs at specific flow velocities governed by the length and shape of the exposed pipeline and is an important source of fatigue damage for both onshore and offshore free spanning pipelines. Reduced velocity V_r is an important parameter in analyzing the onset of vortex shedding-induced oscillations for both in-line and cross-flow motions and and is defined as,

$$V_r = \frac{V}{f_n D} \tag{2.2}$$

where f_n is the natural frequency of vibration of pipe, V is the actual velocity of river water and D is the outer diameter of the pipe.

When the river velocity is low, symmetric vortices are shed and the pipe begins to oscillate in-line with the flow when the vortex shedding frequency equals to about one-third the natural frequency of the pipe span. In-line VIV occurs in two distinct instability regions. The amplitude of in-line VIV increases with reduced velocity in the first region and the amplitude almost remains constant in the second instability region. Reduced velocity typically varies between 1 and 2.2 in the first instability region and varies between 2.2 and 4.5 in the second instability region.

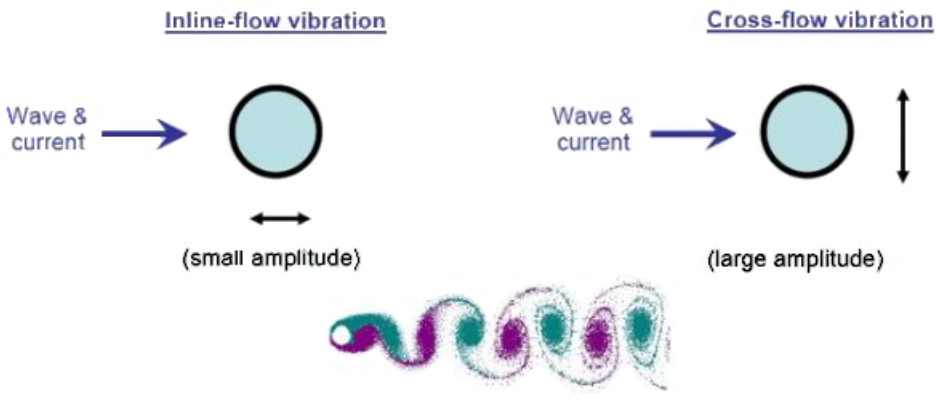

Figure 2.2: Vortex Induced Vibration of a pipe due to its interaction with flowing water.
Note. Reprinted from [2]

At higher velocities, the Reynold's number increases and the flow becomes asymmetric resulting in motion transverse to the flow due to the development of different lift forces on either side of the pipe. Cross-flow VIV typically occurs at reduced velocities between 3 and 5. The exact transition from in-line second stability region to the onset of cross-flow vibrations is difficult to determine.

2.4 Existing methodologies for estimating Critical Span Length

Over many years, various research papers, design codes and industry publications have come up with different analysis and methods to determine Critical Span Length or Maximum Allowable Free Span Length (MAFSL) for pipelines. The Combined Analysis Method prescribes various static and dynamic analysis methods, addressing different loading conditions on the pipe span which are listed below as follows [21]:

1. Static Analysis of free spans induced by low depressions.
2. Static Analysis of free spans using simple beam relations based on ASME B31.8 codes.
3. Static Analysis of free spans induced by elevated obstructions.
4. General Dynamic VIV Analysis.
5. Analysis of Cross-flow VIV based on DNV Guidelines.

2.4.1 Static Analysis

The static analysis of free spans induced by low depression accounts for loads such as dead weight of the pipeline and contents causing severe bending stresses resulting in sagging at the middle of the pipe span. This method calculates MAFSL using the criteria of bending stress. In the second method, the pipe is modelled as a beam and the MAFSL is calculated using the longitudinal and combined stress limitations based on either Maximum Shear Stress theory or the Maximum Distortional Energy Theory (Von Mises combined stress) prescribed by ASME B31.8 regulations. Static analysis of free spans induced by elevated obstructions is similar to that of free spans induced by low depressions except that residual tension is taken into consideration in the former case.

2.4.2 Dynamic Analysis

The general dynamic analysis for VIV in free spanning pipelines is based on limiting the reduced velocity between 3.0 and 5.0, which corresponds to the onset of cross-flow VIV. The limiting criteria for MAFSL is derived from the following relation [22]:

$$f_s < 0.7 f_n \tag{2.3}$$

where f_s is the vortex shedding frequency calculated based on Strouhal number and f_n is the natural frequency of vibration of the pipe. The probability of cross-flow VIV can be minimized when the vortex shedding frequency around the pipe is less than 70% of the natural frequency of the pipeline. Strouhal number is assumed to be 0.2 and the free span end fixity constant is taken as 2.52 assuming that the pipelines are partially fixed and supported [12]. The final methodology prescribed for the analysis of cross-flow VIV is based on the limit state and partial safety factor design criteria where safety class factor (ψ_T), period transformation factor (ψ_D), natural frequency reduction factor (ψ_R) and extreme current variability factor (ψ_U) are taken into account for estimating Maximum Allowable Free Span Length.

The output from all of these methods are compared and the most conservative or minimum value is chosen as the critical span length.

2.4.3 Influence of Internal fluid pressure on Critical Span Length

There have been lots of studies to further understand how internal pressure influences the natural frequency of vibration of pipeline. Olav Fyriliev and Leif Collberg explained how both buoyancy (external pressure) and weight of internal fluid (internal pressure) have an indirect effect on the effective axial force which is mathematically modelled into a differential equation using Hoop stress and Poisson effect [23]. Though DNV-RP-F105 provides some guidance on the critical buckling load and natural frequency of vibration of pipeline based on internal and external

pressure, the non-linear effects due to gradual pipeline deflection are not exactly modelled and expressions based on linear beam theory shall not be valid for all cases.

2.4.4 Influence of Soil Stiffness on Critical Span Length

In order to understand the effects of soil characteristics on the natural frequency of vibration, the pipe-soil interactions were simulated using vertical and horizontal springs, that would prevent pipe oscillations in the cross-flow and in-line directions respectively [15]. DNV proposed simplified formulae for calculating dynamic lateral and vertical soil stiffness (equations 3.4 and 3.5) based on the assumption that the soil is non-stratified and homogeneous. Finite Element Modeling and simulations were also carried out in ABAQUS with various boundary conditions. It was observed that dense sand with pinned/pinned boundary condition had maximum influence on the natural frequency of vibration and soft clay soil with fixed/fixed end condition had minimal influence on the natural frequency.

Hence, we can clearly see the governing factors which affect the critical span length changes for each loading case, and there are difficulties in mathematically modeling the physics of the free span scenario by considering all environmental parameters associated with pipelines. This thesis is an attempt to understand the effect of these variables on MAFSL through historical data and non-linear estimations using Artificial Neural Networks.

3. DATA PREPARATION

The factors that govern the scour depth and maximum allowable free span length of river crossing pipelines are multi-fold in nature. The exact relationships between them have not been identified completely and hence we resort to ANN to develop a robust prediction model. The task of extracting relevant features from available data in a measurable form is quite challenging and is a study of its own by itself. In this chapter, we highlight the process of determining suitable features that are measurable from various data sources available online.

3.1 PHMSA Database

Pipeline and Hazardous Material Safety Administration (PHMSA) of the U.S. Department of Transportation (DOT) has been responsible for collecting oil and gas pipeline related data and incident reports in the United States from the early 1970's, and have made them publicly accessible online. Over many years, several modifications and regulations were established from time to time regarding the way in which pipeline incidents had to be reported. Hence, the data may be found to be temporally inconsistent with respect to the reporting criteria. The definition of an "accident" has changed over time and for this reason, several accidents in the late 20th century and early 21st century were not included in the dataset as they did not meet the criteria of an accident at that time.

PHMSA has been continuously increasing the quality and quantity of information that is being made available to the public. The National Pipeline Mapping System (NPMS) Public Map Viewer, a web based mapping application that serves public with displaying and querying data including attributes related to gas transmission and hazardous liquid pipelines, functions under the jurisdiction of PHMSA. Figure 3.1 indicates the map of Harris county in Texas as seen via NPMS Public Map Viewer. The blue lines represent the Gas Transmission Pipelines and the red lines represent Hazardous Liquid Pipelines. The violet and the green dots in the map indicate accidents that occurred at those locations in Hazardous Liquid pipelines and Gas Transmission pipelines respectively. As a user can controls the position of the cursor, he / she can obtain the latitude and longitude infor-

mation for each point displayed in the mapping system. The NPMS Viewer allows the user to view the pipeline routes one county at a time. One can also access the location of Liquefied Natural Gas (LNG) plants and breakout tank data for every county in the U.S. through this mapping system.

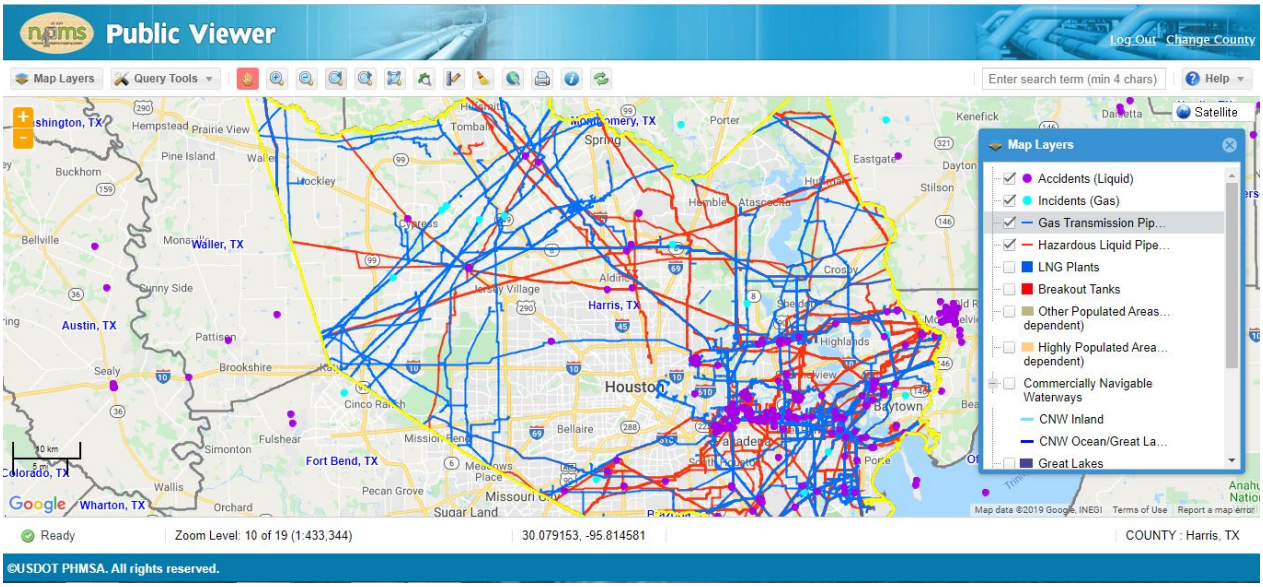

Figure 3.1: NPMS Public Viewer for Harris County, Texas

This study considers all onshore river crossing gas transmission and hazardous liquid pipelines in the U.S., regulated by PHMSA subject to failure by VIV loading during floods from 1986. Factors including Pipeline Outer Diameter (OD), Wall Thickness (WT), Yield Strength (SMYS), Pipe material, Internal fluid pressure (P) inside the pipe, and Age of pipe from its installation year are all captured from the corresponding incident reports in the PHMSA database. Apart from these factors, the latitude, longitude and time of pipeline failure are stored separately in order to reference other databases to capture the associated river and soil properties of the incidents.

3.2 River Stage and Discharge rates - USGS and NOAA

The United States Geological Survey (USGS) and the National Oceanic and Atmospheric Administration (NOAA) monitor real time discharge rates and water levels/stages for various rivers and streams by setting up a network of streamgages and stations across the United States. The

Advanced Hydrological Prediction Service under the NOAA provide river hydrograph mappings that indicate the peak discharge rate during floods at various times in history. For each incident, based on the latitude and longitude from the PHMSA database, we capture river depth, discharge rate (Q) and in turn river velocity at four different times including the peak velocity occurrence during the flood event.

3.3 Data for Dynamic Lateral and Vertical Soil Stiffness values

Modeling of pipe-soil interactions is essential for evaluating the static equilibrium configuration and dynamic response of a free spanning pipeline. The lateral (horizontal) dynamic stiffness K_L is defined as the dynamic horizontal force between pipe and soil per unit length of pipe. The vertical dynamic stiffness K_V is defined as the dynamic vertical force between pipe and soil per unit length of pipe. The two parameters K_L and K_V for non-stratified and homogeneous soil are determined based on the DNV Recommended practice for Free Spanning Pipelines [7], which are as follows

$$K_V = \frac{C_V}{1-\nu}(\frac{2\rho_s}{3\rho} + \frac{1}{3})\sqrt{D} \tag{3.1}$$

$$K_L = C_L(1+\nu)(\frac{2\rho_s}{3\rho} + \frac{1}{3})\sqrt{D} \tag{3.2}$$

, where C_L and C_V are coefficients selected based on Table 3.1, ν is the Poisson's ratio and equals 0.5 for undrained conditions, ρ_s / ρ represents the specific mass ratio between the pipe mass and the displaced water and D is the pipe outer diameter in meters. Density of steel equals 7861 kg/m^3. Density of fluid inside the pipeline ia taken as 870 kg/m^3 for light crude oil and 0.8 kg/m^3 for natural gas. The above stiffness parameters K_L and K_V play a crucial role in modeling pipe-soil interactions to determine the natural frequency of vibration of the pipe. The soil type is identified by the value of its friction angle, which is a characteristic parameter of the soil. Typical friction angles for different types of sand are given in Table 3.2.

Soil type	$\mathbf{C}_V$ (kN/m$^{(5/2)}$)	$\mathbf{C}_L$ (kN/m$^{(5/2)}$)	$\mathbf{K}_{V,S}$ (kN/m/m)
Loose sand	10500	9000	250
Medium sand	14500	12500	530
Dense sand	21000	18000	1350

Table 3.1: Dynamic stiffness factor and static stiffness values for pipe-soil interaction in sand. *Note.* Adapted from [7]

The Natural Resources Conservation Service (NRCS) under the United States Department of Agriculture provides soil maps and data surveyed throughout the United States as a web based application to the public. Based on the river, the latitude and longitude of the pipeline incident, the contents of sand on the pipeline shoulders are identified to determine its friction angle and in turn the coefficient values. Using this method, the lateral and vertical dynamic soil stiffness values are determined for all the pipeline incidents.

Soil type	ψ_s
Loose sand	28 - 30^o
Medium sand	30 - 36^o
Dense sand	36 - 41^o

Table 3.2: Typical Friction angles for sand. *Note.* Adapted from [7]

3.4 Estimation of Reduced velocity

3.4.1 In-line oscillation

The in-line response of a pipeline span in current dominated conditions is associated with either alternating or symmetric vortex shedding. The onset of in-line VIV can be analyzed from the plot between reduced velocity (V_r) and stability parameter (K_s) as shown as Figure 3.2. The dimensionless stability parameter plays a significant role in assessing in-line vortex induced motion and is calculated as follows

$$K_s = \frac{2M_e\delta}{\rho D^2} \tag{3.3}$$

, where M_e is the effective mass and equals the sum of mass of pipe, its contents and added mass, δ is the logarithmic decrement of structural damping and equals 0.125 for steel, ρ is the density of fluid around the pipe and D is the pipe outer diameter.

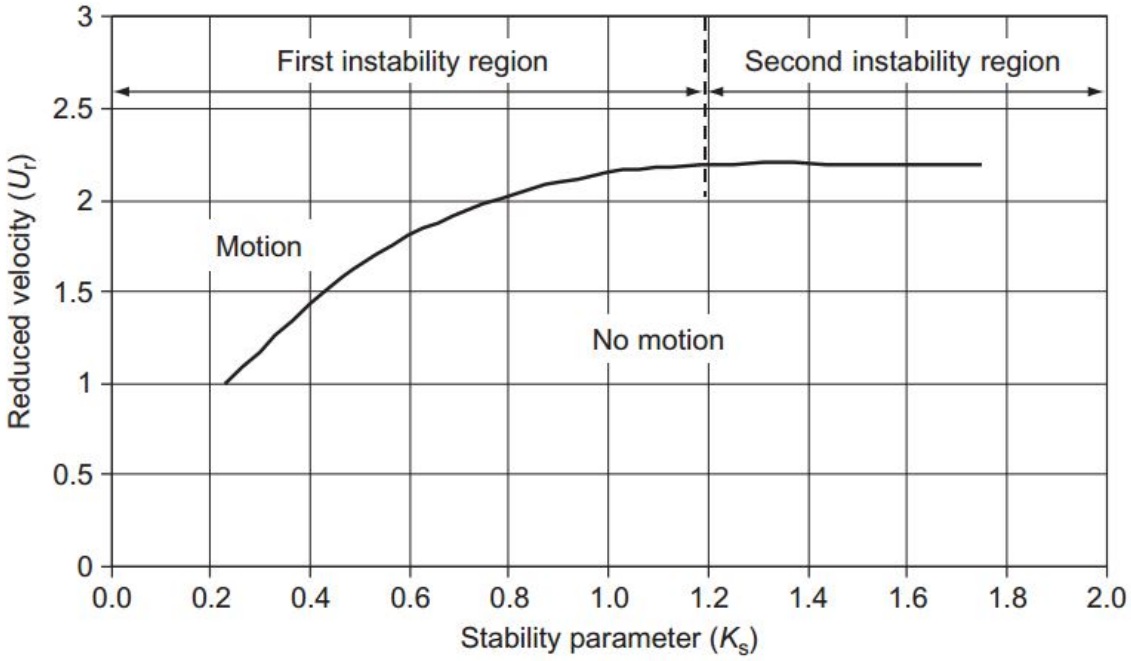

Figure 3.2: Reduced velocity for In-line oscillations based on Stability parameter K_s.
Note. Reprinted from [3]

The mathematical function representing the relation between reduced velocity and stability parameter in the first and second instability region is given by equation 3.4, which can be found in Chapter 11, Handbook of Offshore Engineering [24].

$$V_r = \begin{cases} 1 & \text{, if } K_s \leq 0.25 \\ 0.188 + 3.6K_s - 1.6K_s^2 & \text{, if } 0.25 < K_s \leq 1.2 \\ 2.2 & \text{, if } K_s > 1.2 \end{cases} \tag{3.4}$$

3.4.2 Cross-flow oscillation

The onset of cross-flow VIV can be estimated from the plot between reduced velocity (V_r) and Reynold's number (R_e) as shown in Figure 3.3, Offshore Pipelines (Second edition, Chapter 5) [3]. Excitations in the cross-flow direction are far more dangerous than in-line when the vortex shedding frequency roughly equals the natural frequency of vibration of pipe span due to higher amplitudes of response and fatigue damage. The mathematical function representing the relation between the two parameters is given by equation (3.5) from Chapter 11, Handbook of Offshore Engineering [24].

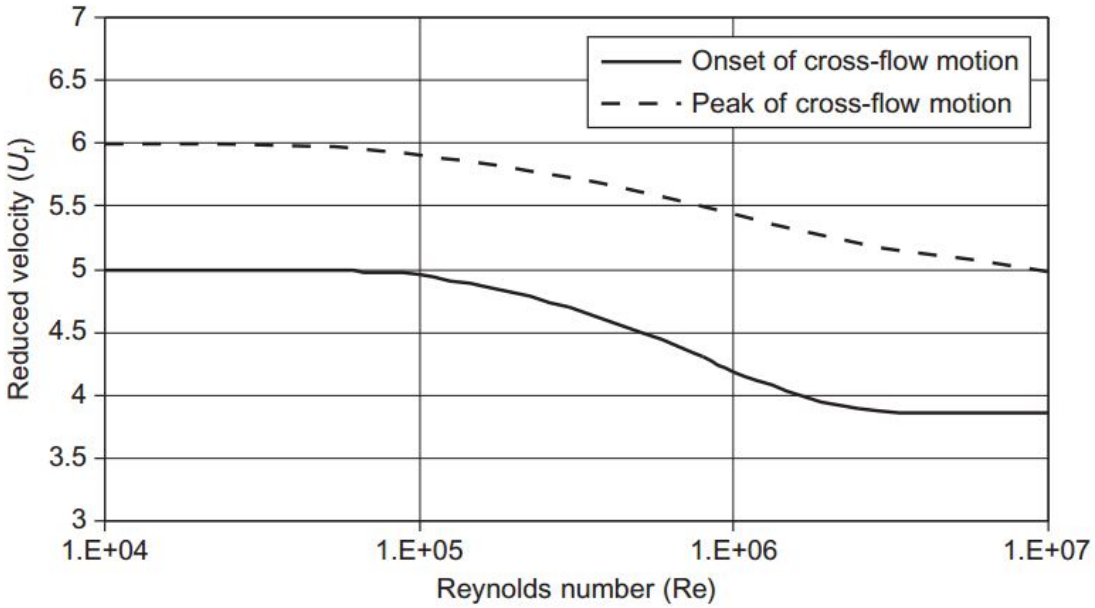

Figure 3.3: Reduced velocity for Cross-flow oscillations based on Reynold's number Re.
Note. Reprinted from [3]

$$V_r = \begin{cases} 5 & \text{, if } Re \leq 5 \times 10^4 \\ c_1 - c_2 Re + c_3 Re^2 + c_4 Re^3 + c_5 Re^4 & \text{, if } 5 \times 10^4 < Re \leq 3 \times 10^6 \\ 3.87 & \text{, if } Re > 3 \times 10^6 \end{cases} \tag{3.5}$$

where $c_1 = 5.07148$, $c_2 = 1.61569 \times 10^{-6}$, $c_3 = 8.73792 \times 10^{-13}$, $c_4 = 2.11781 \times 10^{-19}$ and $c_5 = 1.89218 \times 10^{-26}$.

3.5 Data cleaning and preprocessing

In summary, we have chosen data corresponding to thirteen input features from various sources available that can distinctly characterize the output parameters that were used in this study. In Machine Learning, data cleaning involves identifying and filtering inaccurate or missing data in a way easier to explore, understand and model for prediction. Any parameter involved in the set of features should be relevant and measurable for the final model to have minimum error and high accuracy during prediction. Incomplete data and non essential features need to be excluded in order to allow our model to generalize well.

3.5.1 Correlation Matrix

Correlation is a statistical measure that indicates the strength and direction of a relationship between a pair of variables. Correlation coefficient between variables X and Y where each pair of data is denoted by (x_i, y_i) is calculated using the following relation:

$$r = \frac{\sum_{i=1}^{n} (Z_x)_i (Z_y)_i}{n-1} \tag{3.6}$$

$$where \quad (Z_x)_i = \frac{x_i - \bar{x}}{s_x} \quad and \quad (Z_y)_i = \frac{y_i - \bar{y}}{s_y} \tag{3.7}$$

Here n represents the total number of ordered pairs in the dataset, $\bar{x}$, $\bar{y}$ indicate the mean of variables, and s_x, s_y represent the standard deviation of the variables X and Y. The correlation coefficient (r) varies between -1 and 1, and is a numerical measure of the degree of association between the variables. Positive coefficients indicate a direct relation between the variables and negative correlations represent an inverse relationship. Correlations above 0.4 are considered to be relatively strong, those between 0.2 and 0.4 are moderate, and values between 0 and 0.2 are considered weak in the positive direction. Similarly, correlations below -0.4 are considered strongly negative, those between -0.4 and -0.2 are moderately negative and values between -0.2 and 0 are considered weakly negative.

S.No	OUTPUT / INPUT	Scour depth	CSL for In-line motion	CSL for Cross flow motion
1	Pipe Outer Diameter (OD)	0.911	0.333	0.495
2	Pipe wall thickness (WT)	0.317	0.415	0.383
3	Yield Strength (SMYS)	0.407	0.136	0.191
4	Internal fluid pressure (P)	0.203	-0.035	0.055
5	River water depth (WD)	0.180	0.102	0.195
6	Age of pipeline installed (years)	-0.048	0.260	0.216
7	Discharge rate (Q)	0.220	-0.125	-0.054
8	Ratio of density of fluid to that of density of pipe material (carbon steel) (ρ/ρ_s)	-0.004	0.230	0.191
9	Ratio of density of water to that of density of pipe material (carbon steel) (ρ_w/ρ_s)	-10^{-17}	10^{-16}	-10^{-16}
10	Reduced velocity for in-line motion (V_r) based on Stability parameter K_s	-0.425	0.074	-0.025
11	Reduced velocity for cross-flow motion (V_r) based on Reynolds number R_e	0.521	0.133	0.341
12	Dynamic Lateral soil stiffness (K_L)	0.394	0.295	0.315
13	Dynamic vertical soil stiffness (K_V)	0.391	0.303	0.324

Table 3.3: Correlation between Input and Output features

Table 3.3 depicts the correlation coefficients between the 13 input parameters and the output features that were identified. We find that there is almost no effect of ratio of density of water to that of pipe material on the output features. Hence, all the remaining 12 parameters have been chosen to model our neural network architecture, as they have relatively moderate or strong correlations with the output features.

4. ARTIFICIAL NEURAL NETWORK MODEL

Computational Intelligence primarily encompasses the family of neural networks, fuzzy logic systems and evolutionary computing to construct data driven models for supplementing or replacing models based on first principles. ANN models have found to be useful and efficient particularly in problems where the characteristics of the processes are difficult to describe using physical equations. Having identified the important input features to predict CSL and Scour Depth from the available datasets, we can proceed to define the ANN architecture as shown in this chapter.

4.1 Overview of Artificial Neural Networks

An Artificial Neural Network (ANN) is a computational model that has the ability to learn and develop transformations or mappings between input and output parameters. It is an efficient technique for solving classification and non-linear regression problems, where the derivation of a mathematical model is not practical. A neural network algorithm is used to determine the relationship between inputs and outputs of a system based on a training dataset that is essentially reflective of the complete behavior inherent in the system. Once a reasonably accurate and representative model is configured, we can perform several analysis methods that can provide us with insights to the problems.

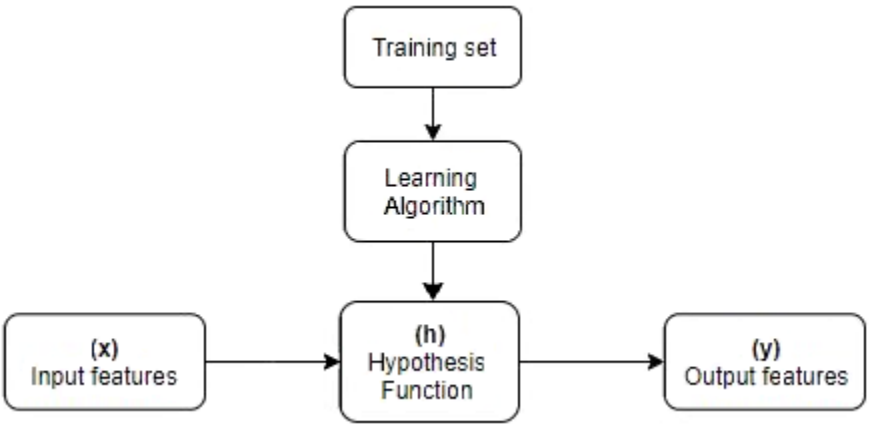

Figure 4.1: Representation of Hypothesis function

4.1.1 Neural Networks Model Representation

Neurons and its associated weights constitute the primary elements of a typical neural network architecture. Neurons within an ANN are basically computational units that can model the functioning of a biological neuron by receiving inputs from various units and translating them into a single output. This output is then fed as an input to another layer of neurons. Let us examine how we can mathematically represent a hypothesis function using neural networks. Given a training set, our objective is to learn a hypothesis function $h : x \rightarrow y$, so that $h_w(x)$ is a good predictor for the corresponding value of our output features y.

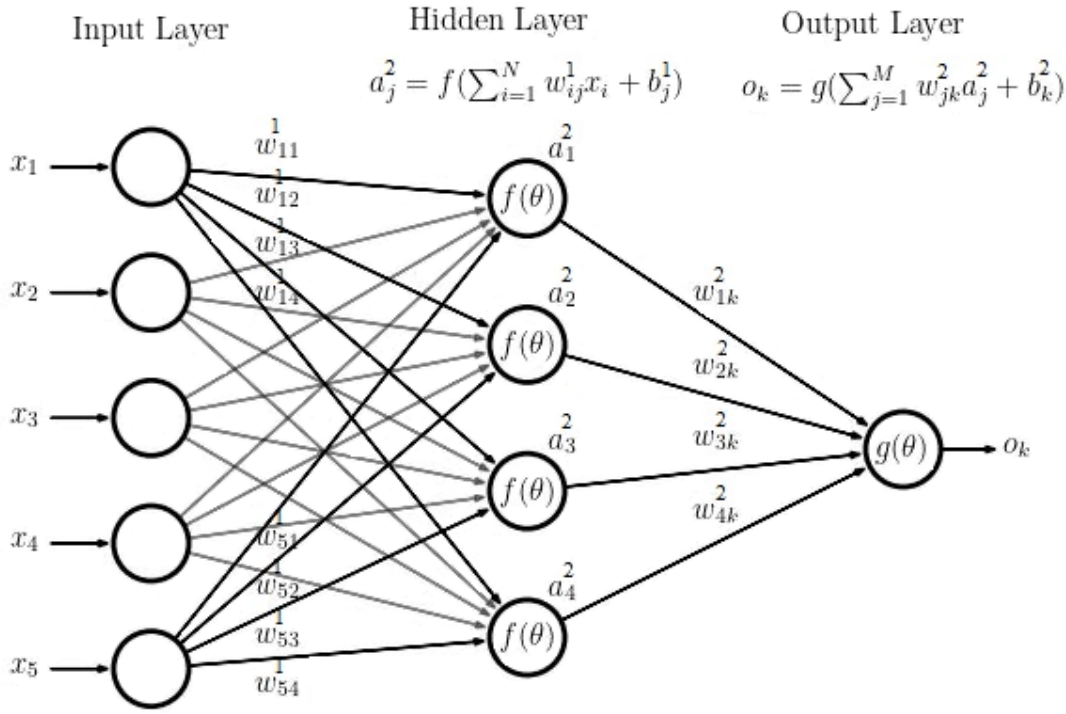

Figure 4.2: A generic neural network architecture with single hidden layer.
Note. Adapted from [4]

Figure 4.2 represents a generic neural network architecture with 5 input features x_1, x_2, x_3, x_4 and x_5, 1 hidden layer with 4 units namely a_1, a_2, a_3 and a_4, and an output layer with 1 unit o_k which is the result of the hypothesis function. Let us define all the variables that are used to model our

hypothesis function:

a^j = matrix of activation units in layer j

a_i^j = activation unit i in layer j

w^j = matrix of weights controlling function mapping from layer j to layer $j+1$.

$w_{i,k}^j$ = element of the w^j weight matrix that maps i^{th} node of layer j and k^{th} node of layer $j+1$.

b^j = weight matrix elements that maps bias unit in layer j to neurons in layer $j+1$.

f = activation function used to compute hidden layer neurons.

g = activation function used to compute neurons in the output layer.

L = Total number of layers in the network including the input and output layer. Here L = 3.

K = Number of output units. Here K = 1.

The values of the activation nodes in the Hidden Layer (second layer of the architecture) can be obtained as follows:

a_0^2 = 1 (bias unit)

a_1^2 = f ($b_1^1 + w_{11}^1 x_1 + w_{21}^1 x_2 + w_{31}^1 x_3 + w_{41}^1 x_4 + w_{51}^1 x_5$)

a_2^2 = f ($b_2^1 + w_{12}^1 x_1 + w_{22}^1 x_2 + w_{32}^1 x_3 + w_{42}^1 x_4 + w_{52}^1 x_5$)

a_3^2 = f ($b_3^1 + w_{13}^1 x_1 + w_{23}^1 x_2 + w_{33}^1 x_3 + w_{43}^1 x_4 + w_{53}^1 x_5$)

a_4^2 = f ($b_4^1 + w_{14}^1 x_1 + w_{24}^1 x_2 + w_{34}^1 x_3 + w_{44}^1 x_4 + w_{54}^1 x_5$)

The neuron in the output layer which is the predicted result of our hypothesis function can be calculated as follows:

o_k = g ($b_1^2 + w_{11}^2 a_1^2 + w_{21}^2 a_2^2 + w_{31}^2 a_{3^2} + w_{41}^2 a_4^2$)

The hypothesis output is essentially the activation function applied to the sum of product of activation nodes and elements of the weight matrix w^j in the last layer. The activation function can be visualized as a transformation that maps the input signals into output signal required for the neural network to function. There are several non-linear activation functions including but not limited to sigmoid, hyperbolic tangents and rectified linear units that can be selected based on the

nature of data, network architecture and model performance.

4.1.2 Back-propagation algorithm

Back-propagation method [25], generally applied to multilayered feedforward neural networks, is a learning procedure used to optimize the parameters in the hypothesis function by minimizing the loss function for obtaining the best prediction model. The loss function can be defined in a way that calculates the error in prediction. The algorithm takes an initial model with random values for weights and updates itself through an iterative process to minimize error while predicting output(s). The algorithm aims to calculate the gradient of the loss function with respect to all the weights using the backward propagation of errors in the network. A slightly modified version of the back-propagation algorithm is discussed in [26], to accelerate the convergence of the network.

4.1.3 Levenberg-Marquardt algorithm

The Neural Network architecture for predicting critical span length and scour depth can be designed using the Deep Learning Toolbox in MATLAB. The Toolbox provides a framework to create, train and analyse neural network models using various in-built algorithms and features. One such algorithm is the Levenberg-Marquardt (LM) method [27] which was developed to optimize non-linear least square error functions by combining the Gradient descent and Gauss-Newton minimization techniques. In the gradient descent method, the sum of the squared errors is reduced by updating the parameters in the steepest descent direction. In the Gauss-Newton method, the sum of the squared errors is reduced by assuming the least squares function as locally quadratic, and finding the minimum of the quadratic. The LM method acts more like a gradient descent method when the parameters are far from their optimal value, and acts more like the Gauss-Newton method when the parameters are close to their optimal value. Since critical span length and scour depth are non-linear functions of several variables, the LM algorithm was found to be best suited for our case.

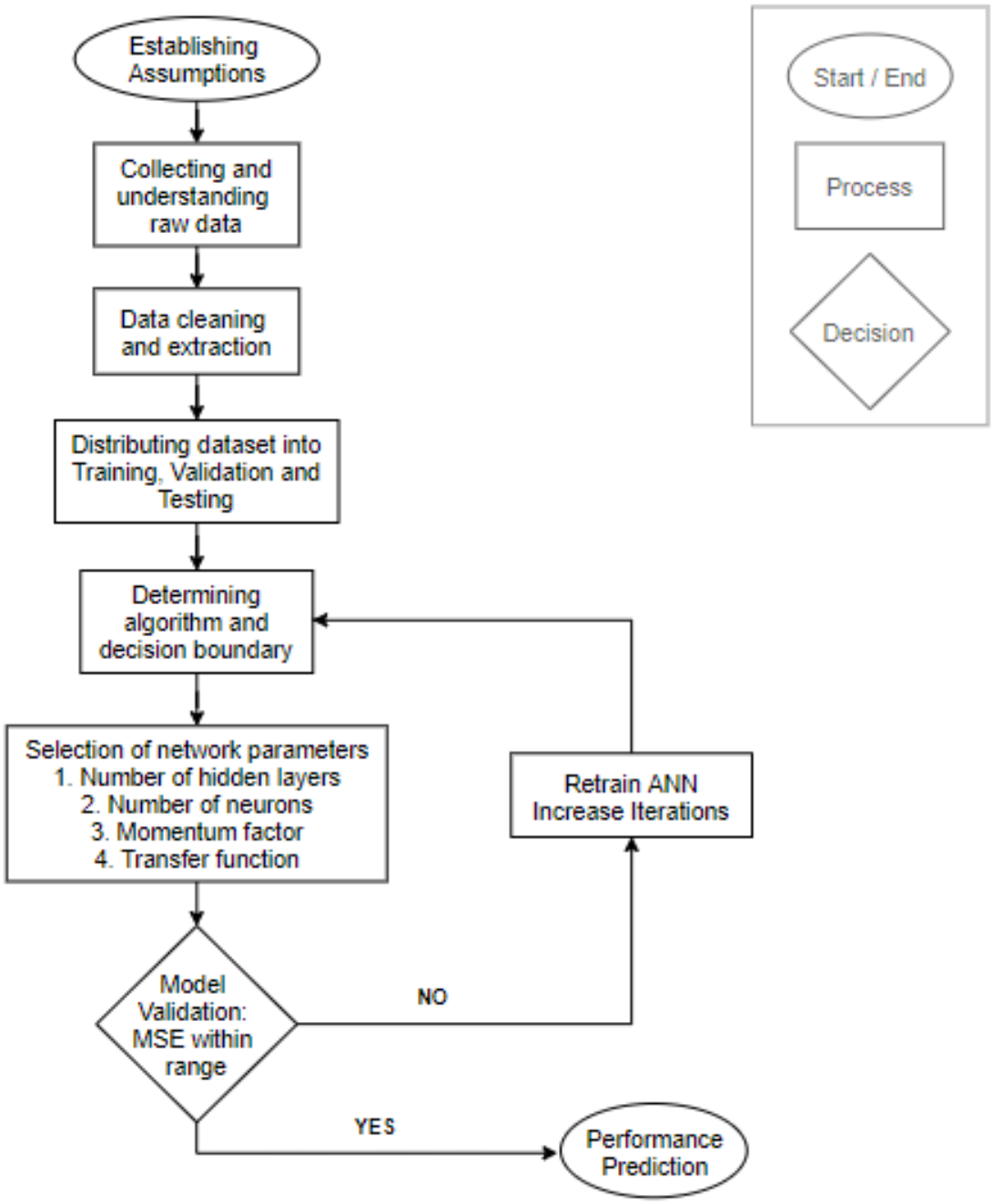

Figure 4.3: Flow chart indicating the procedure for developing an ANN predictive model

4.2 Establishing Assumptions for Model Formulation

The model formulation during this study needed certain key assumptions to be made to predict CSL and scour depth which are listed as follows:

i. The pipelines are situated perpendicular to the flow, where maximum hydrodynamic loads and vortex induced vibrations would be expected.

ii. The pipeline under study is on the river bed and hence scouring will expose the pipeline and induce VIV, when flooding occurs.

iii. The soil on the pipe shoulder is assumed to be non-stratified and homogeneous in all the cases for calculating lateral and vertical dynamic soil stiffness as there are no standard prescriptions for computing stiffness values for heterogeneous soils.

iv. The free span end fixity constant is 1.57 for pinned/pinned ends and 3.54 for fixed/fixed ends. In this study, we have considered the value to be 2.52 for all cases because in reality, pipes are neither completely pinned nor clamped on the ends.

v. The cross sectional area of the river is taken as the product of width and depth, and the river water is assumed to flow at mean velocity when it comes in contact with the pipe neglecting the variation of velocity with depth.

4.3 Identifying Input and Output features for the Network

Forty five incidents were captured from the PHMSA database pertaining to failure of gas transmission and hazardous liquid pipelines as a result of VIV loading due to floods in the last 35 years. For each of the forty five incident cases, river velocity, discharge rate and river stage were captured at four different times resulting in a total of 180 analyzed data sets.

Table 4.1 indicates the twelve input parameters that were identified for modelling the neural network. Our input data can be represented as a 180×12 matrix, where 180 depicts the number of samples and 12 depicts the number of features for every sample. Scour depth parameters were evaluated for all the 180 data sets using the Froude Number approach as prescribed by Moncada and Aguirre-Pe [20]. First general formulations of DNV on calculations of critical span lengths due to inline and cross flow oscillations were carried out for all the cases. The critical span length calculations for all the incidents were validated based on the approach prescribed by Minerals Management Service under United States Department of the Interior [21].

S.No	Parameters	Units
1	Pipe Outer Diameter (OD)	inches (in)
2	Pipe wall thickness (WT)	inches (in)
3	Yield Strength (SMYS)	pounds per square inch (psi)
4	Internal fluid pressure (P)	psig (gauge pressure)
5	River water depth (WD)	feet (ft)
6	Age of pipeline installed	years
7	Discharge rate (Q)	Cubic feet per second (ft^3/sec)
8	Ratio of density of fluid to that of density of pipe material (carbon steel) (ρ/ρ_s)	-
9	Reduced velocity for inline oscillations (V_r) based on Stability parameter K_s	feet per second (ft/sec)
10	Reduced velocity for crossflow oscillations (V_r) based on Reynolds number R_e	feet per second (ft/sec)
11	Dynamic Lateral soil stiffness (K_L)	lbf/ft^2
12	Dynamic vertical soil stiffness (K_V)	lbf/ft^2

Table 4.1: Input Features for modeling Neural Network Architecture.

Hence our output data can be represented as a 180×3 matrix, where 180 depicts the number of samples and 3 depicts the number of output parameters for every sample namely scour depth, critical span length due to inline oscillation and critical span length due to cross flow oscillation.

4.3.1 Feature Scaling

Feature scaling involves dividing the input values of one or more attributes by the maximum value of that particular attribute, resulting in a new range between 0 and 1. Unlike normalization, feature scaling does not alter the distribution of the data and only re-scales the data to the desired range. A good reason to perform features scaling is to ensure that one attribute doesn't dominate others. We can speed up the process of gradient descent by having each of our input values in roughly the same range. The error decreases rapidly after every iteration and the model converges quickly when the input features are re-scaled. The weight matrices will oscillate inefficiently when the variables are uneven and have large ranges.

4.4 Determining the best fit Artificial Neural Network model

Feature scaling was performed to selective attributes such as yield strength, internal fluid pressure, discharge rate and dynamic lateral and vertical soil stiffness values to ensure all the input attributes had values in a similar range. The 180 data sets were then split into 3 categories namely Training, Validation and Testing in the ratio 15:2:3 which was determined by trial and error through interactive tests. The schematic diagram of the Neural Network architecture designed by using Deep Learning Toolbox in Matlab is depicted in Figure 4.4. The architecture comprised of a back-propagation network with 2 hidden layers having 30 neurons each and the input layer having 12 neurons corresponding to the 12 features. The network was trained for various numbers of iterations using the Levenberg-Marquardt (LM) algorithm. Based on the analysis of Mean Square Error (MSE) for training, validation and testing data sets, the best model was chosen that generalizes well. The performance of the model is discussed in the next chapter.

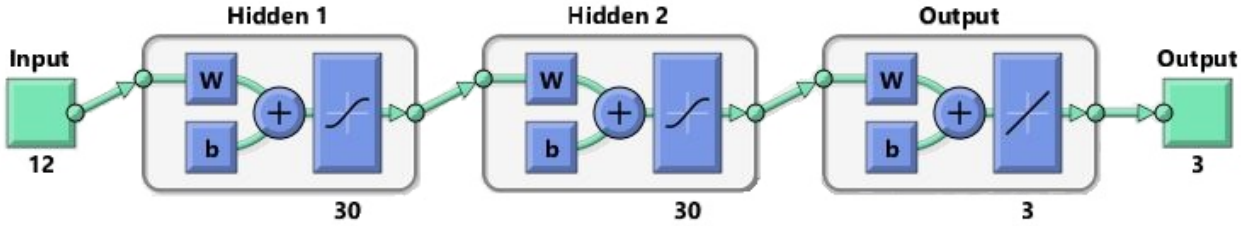

Figure 4.4: Neural Network Architecture

5. RESULTS AND ANALYSIS

The prediction results of the ANN model are analysed in this chapter. The number of hidden layers, neurons, transfer functions and training algorithm were determined in an iterative manner based on the model performance. Table 5.1 summarizes the design parameters of the network architecture used to train the model.

Number of input parameters	12
Number of hidden layers	2
Number of neurons in each hidden layer	30
Number of output parameters	3
Total number of data points	180
Data Division	15:2:3
Number of Training data points	135
Number of Validation data points	18
Number of Testing data points	27
Training Algorithm	Levenberg-Marquardt (trainlm)
First hidden layer Transfer function	Hyperbolic tangent sigmoid (tansig)
Second hidden layer Transfer function	Hyperbolic tangent sigmoid (tansig)
Output layer Transfer function	Linear transfer function (purelin)

Table 5.1: Model results and Network Architecture

The hyperbolic tangent sigmoid (tansig) transfer function is the mathematical equivalent of **tanh** function and can be represented as follows:

$$tansig(N) = \frac{2}{1 + \exp\left(-2 \times N\right)} - 1 \tag{5.1}$$

The symmetric nature of the tansig function enables faster learning of the model when compared to other activation functions. For the output neuron(s), the most appropriate activation function for a feedforward neural network is a linear transfer function (purelin), as it reduces the loss in accuracy of the model when hyperbolic tangent sigmoid transfer function is applied to normalized data in the hidden layers.

5.1 Performance Evaluation

The Performance function plays a crucial role in analyzing the speed and accuracy of the learning network. Here, the Mean Squared Error (MSE) is chosen as the performance evaluation function for the model. MSE is a statistical function which measures the average squared difference between the estimated values and actual value. MSE is always positive, and values closer to zero indicate better performance.

$$MSE = \frac{1}{n}\sum_{i=1}^{n} \mid \overline{Y_i} - Y_i \mid^2 \tag{5.2}$$

Here **n** represents the number of samples in the dataset, $\overline{Y_i}$ and Y_i indicate predicted value and target value of the i^{th} sample respectively. The MSE for Training, Validation and Testing datasets after each iteration (epochs) is shown in Figure 5.2. The **y** axis is logarithmically scaled to clearly interpret the variations in MSE as it goes below 10^{-1}. The MSE for training dataset decreases continuously with the increase in number of iterations and reaches the target of 10^{-3} after the 18^{th} iteration. The MSE for validation dataset decreases for 11 iterations, and gradually increases thereafter. The iteration where least MSE is observed for the validation dataset is selected as the best model. This occurs after the 11^{th} iteration with a MSE of 0.0129. Models from 12^{th} iteration onwards are considered to overfit the training data. The results of the mean squared error for training, validation and testing data set is given in Table 5.2.

Performance analysis	Mean Squared Error (MSE)
Target MSE for Training dataset	0.001
Number of iterations	18
Best performance observed	11^{th} iteration
Overall MSE at best performance	0.0186
Training dataset MSE	0.0041
Validation dataset MSE	0.0129
Testing dataset MSE	0.095

Table 5.2: Mean Squared Error Results

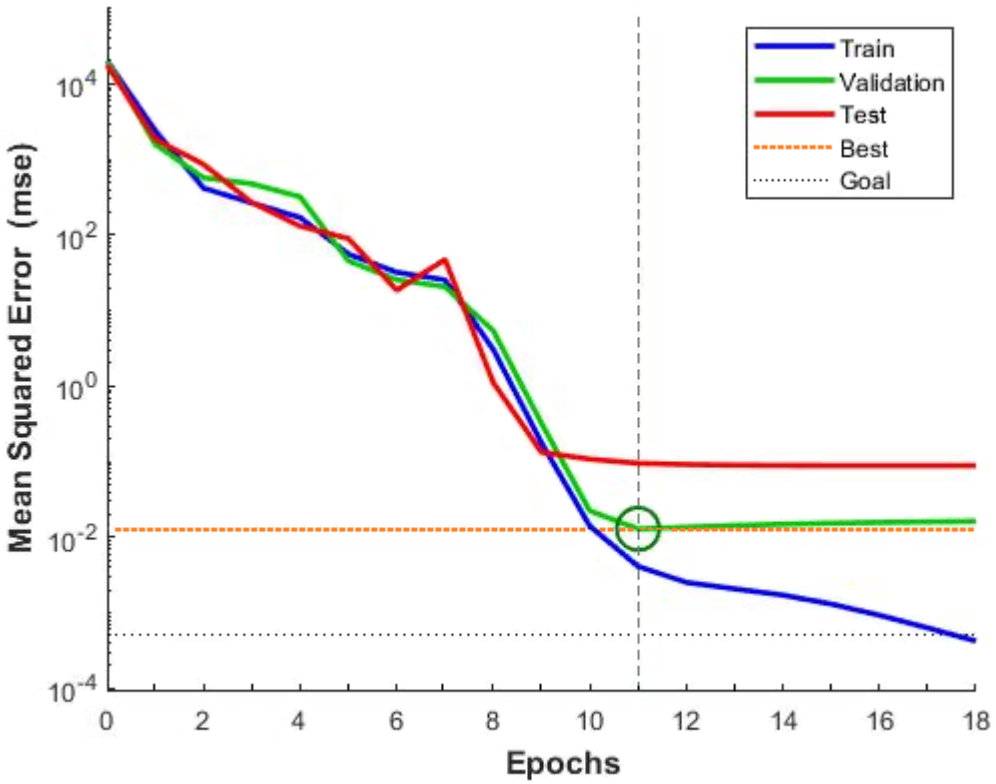

Figure 5.1: Neural Network Performance

5.2 Error Histogram

Figure 5.3 helps us visualize errors between the target values and predicted values for all 180 datasets after training our feedforward neural network. The histogram categorizes the 540 error values into 20 bins with orange line indicating zero error. Percentage error distribution for training, validation and testing dataset is given in Table 5.3. We see that 92% of predicted outputs in the validation dataset and 94% of predicted outputs in the testing dataset have less than 1% error when compared to theoretical results. The errors of the remaining outputs are also less than 4%.

Percentage Error	Training data	Validation data	Testing data
< 0.5	90%	83%	77%
$0.5 \sim 1$	8%	9%	17%
$1 \sim 4$	2%	7%	6%

Table 5.3: Percentage error of predicted outputs in various datasets

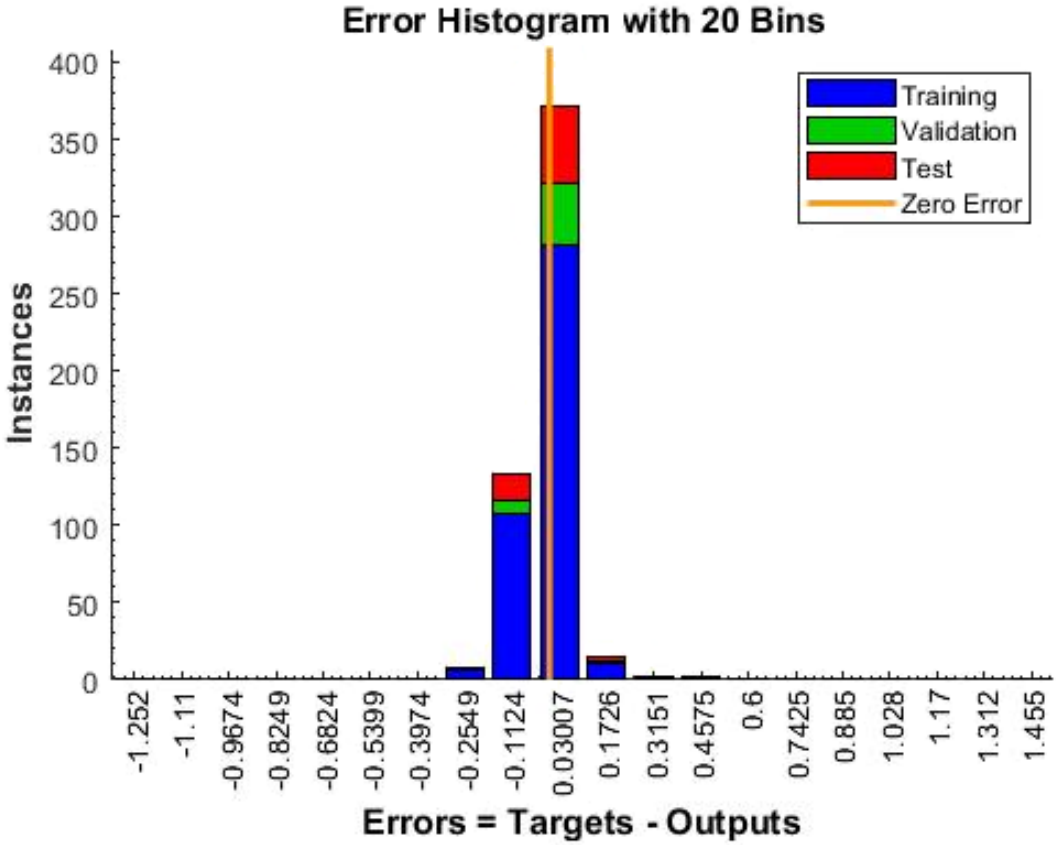

Figure 5.2: Neural Network Error Histogram

Table 5.4 indicates the percentage error distribution for training, validation and testing datasets corresponding to each output feature.

Output variable	Percentage Error	Training set	Validation set	Testing set
Scour depth	< 0.5	96.3%	77.78%	81.48%
	$0.5 \sim 1$	2.22 %	11.11%	11.11%
	$1 \sim 4$	1.48%	11.11%	7.4%
Critical Span Length for Inline oscillations	< 0.5	82.22%	83.33%	85.18%
	$0.5 \sim 1$	15.56 %	11.11%	11.11%
	$1 \sim 4$	2.22%	5.55%	3.7%
Critical Span Length for Cross flow oscillations	< 0.5	91.11%	88.89%	81.48%
	$0.5 \sim 1$	6.67 %	5.56%	11.11%
	$1 \sim 4$	2.22%	5.56%	7.4%

Table 5.4: Percentage error of predicted outputs in various datasets

5.3 Regression Plots

Regression plots indicate the relationship between actual values and the predicted values for the chosen set of data points. The values of the correlation coefficient **R** between target and predicted values for training, validation, and testing data sets as seen in figure 5.4 indicate an accurate prediction of the output values and hence validate the Artificial Neural Network model.

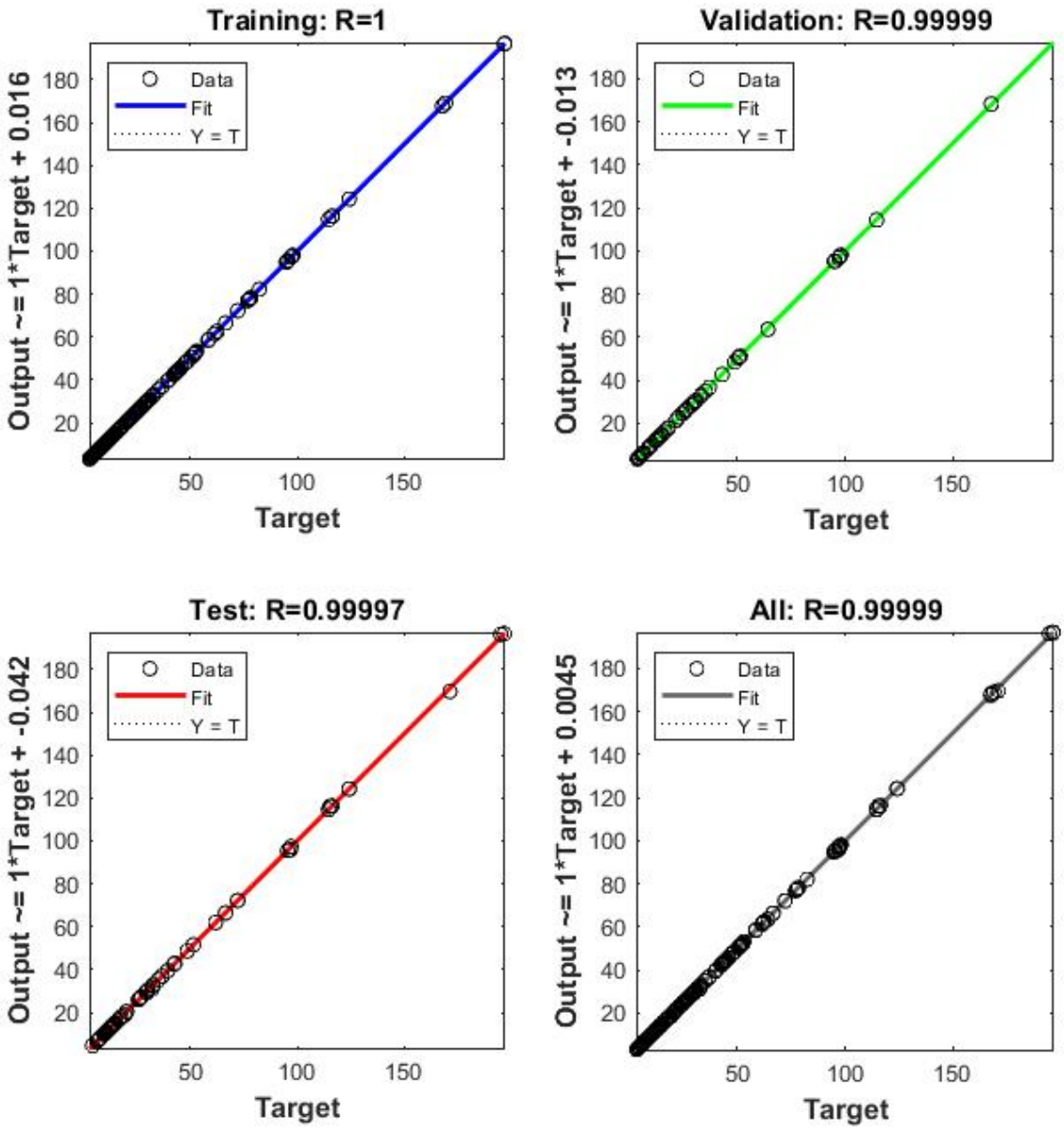

Figure 5.3: Neural Network Regression plots

5.4 Training State Plots

Training state plots indicate how the control parameters vary with iterations. From the various plots in Figure 5.5, we can observe the gradient value to decrease gradually indicating that the error function is reaching its minimum. **Mu** is referred to as the Momentum parameter which is included in weight update function to avoid the problem of local minima. It is approximately equal to the inverse of the Hessian matrix. And finally, from the third plot between Validation checks and iteration, we can see that the validation dataset MSE increases continuously after the 11^{th} iteration, an indication that the minimum MSE has been achieved.

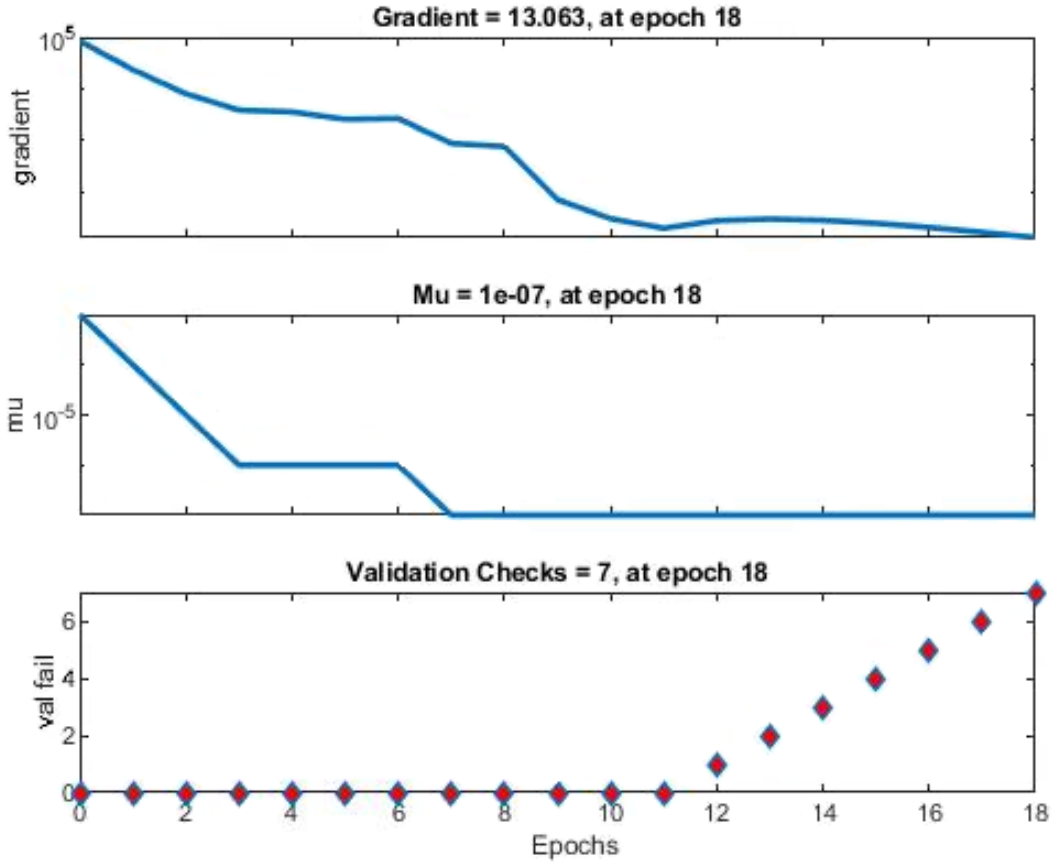

Figure 5.4: Neural Network Training state plots

5.5 Quantifying variable importance in the ANN model

ANN is a powerful statistical technique which captures the relationship between the variables which cannot be easily described by a simple mathematical model. Although ANN provides little explanatory insight into the explicit relation between the independent variables in the prediction process, the Connection Weight Approach provides an excellent methodology for quantifying the importance of the input variables in a neural network [6]. This method calculates the product of the raw input-hidden-output connection weights between each input neuron and output neuron and sums the products across all hidden neurons. The final weights are then used to rank the relative importance of the input features for each output variable.

	Overall Connection Weights		
Input features	**Scour depth**	**CSL for In-line motion**	**CSL for Cross - flow motion**
Pipe Outer Diameter (OD)	1.9065	0.0017	-1.7096
Pipe wall thickness (WT)	-1.4472	3.4527	4.5148
Yield Strength (SMYS)	2.6710	-2.0436	-0.3391
Internal fluid pressure (P)	-2.7444	2.1488	2.4199
River water depth (WD)	0.9861	0.6742	2.7356
Age of pipeline installed	0.6202	0.3790	-1.5626
Discharge rate (Q)	4.6140	-5.3632	-8.6657
Ratio of density of fluid to that of density of pipe material (carbon steel) (ρ/ρ_s)	-0.2113	-1.5621	-3.6170
Reduced velocity for in-line oscillations (V_r) based on Stability parameter K_s	-2.7848	-2.2970	-4.1525
Reduced velocity for cross flow oscillations (V_r) based on Reynolds number R_e	-2.7802	10.3404	9.6695
Dynamic lateral soil stiffness (K_L)	-1.2680	0.3035	3.4515
Dynamic vertical soil stiffness (K_V)	1.7570	0.4750	-3.4983

Table 5.5: Overall Connection Weights of Input parameters based on Olden's approach.
Note. Adapted from [8]

In order to better understand the interactions between variables, the strength and direction of each connection weight within the network must be examined directly. A weight decides how much influence the input will have on the output. Weights near zero imply changing this input will not significantly affect the output. Negative weights mean increasing this input will decrease the output. The relative importance of an input variable in estimating an output variable is computed as a percentage of magnitude of its overall connection weight with respect to the summation of absolute values of overall connection weights of all input variables.

Rank	**Scour depth prediction**	
	Relative Importance	**Input feature**
1	19.4%	Discharge rate (Q)
2	11.71%	Reduced velocity for in-line oscillations (V_r) based on Stability parameter K_s
3	11.69%	Reduced velocity for cross-flow oscillations (V_r) based on Reynolds number R_e
4	11.54%	Internal fluid pressure (P)
5	11.2%	Yield Strength (SMYS)
6	8.0%	Pipe Outer Diameter (OD)
7	7.4%	Dynamic vertical soil stiffness (K_V)
8	6.1%	Pipe wall thickness (WT)
9	5.3%	Dynamic lateral soil stiffness (K_L)
10	4.1%	River water depth (WD)
11	2.6%	Age of pipeline installed
12	0.8%	Ratio of density of fluid to that of pipe material (carbon steel) (ρ/ρ_s)

Table 5.6: Relative importance of input parameters in predicting scour depth

Table 5.6 displays the relative order of input features used in ANN to estimate scour depth. Moncada and Aguirre-Pe used river velocity, water depth and pipeline outer diameter in their derivation of empirical relationship to estimate scour depth [20]. Here, we see that factors such as internal fluid pressure, yield strength, pipe wall thickness, dynamic vertical and lateral soil stiffness are also statistically significant in terms of weights and play a crucial role in the prediction process.

Rank	CSL for in-line motion		CSL for cross-flow motion	
	Relative Importance	**Input feature**	**Relative Importance**	**Input feature**
1	35.6%	Reduced velocity for cross flow oscillations (V_r) based on Reynolds number R_e	20.9%	Reduced velocity for cross flow oscillations (V_r) based on Reynolds number R_e
2	18.5%	Discharge rate (Q)	18.7%	Discharge rate (Q)
3	11.9%	Pipe wall thickness (WT)	9.7%	Pipe wall thickness (WT)
4	7.9%	Reduced velocity for inline oscillations (V_r) based on Stability parameter K_s	8.9%	Reduced velocity for inline oscillations (V_r) based on Stability parameter K_s
5	7.4%	Internal fluid pressure (P)	7.8%	Ratio of density of fluid to that of pipe material (carbon steel) (ρ/ρ_s)
6	7.0%	Yield Strength (SMYS)	7.5%	Dynamic vertical soil stiffness (K_V)
7	5.4%	Ratio of density of fluid to that of pipe material (carbon steel) (ρ/ρ_s)	7.4%	Dynamic lateral soil stiffness (K_L)
8	2.3%	River water depth (WD)	5.9%	River water depth (WD)
9	1.6%	Dynamic vertical soil stiffness (K_V)	5.2%	Internal fluid pressure (P)
10	1.3%	Age of pipeline installed	3.7%	Pipe Outer Diameter (OD)
11	1.05%	Dynamic lateral soil stiffness (K_L)	3.4%	Age of pipeline installed
12	0.006%	Pipe Outer Diameter (OD)	0.7%	Yield Strength (SMYS)

Table 5.7: Relative importance of input parameters in predicting Critical Span Length

Table 5.7 shows the relative order of input features used to estimate Critical Span Length due to in-line as well as cross-flow motion. We observe that factors such as reduced velocities based on reynold's number and stability parameter, discharge rate, pipe wall thickness and internal fluid pressure have high relative importance in both cases. Dynamic vertical and lateral soil stiffness values also have significant statistical contribution in terms of weights. Hence, we can conclude that this approach results in the correct identification of variable contribution as it computes the relative importance using raw weights and accounts for the direction of the input-hidden-output relationship.

5.6 Pipeline Vulnerability assessment using the ANN model

A screening level evaluation of vulnerability of pipelines at water crossings is performed by comparing MAFSL and the maximum exposure length of the watercourse based on its geomorphic properties. The vulnerability can be characterized using Free Span Ratio (FSR), which is defined as the ratio of MAFSL to the maximum exposure length [28]. For the purpose of calculation, a convenient assumption made is to use the bankfull width (L_{bfw}) of the water crossing in place of the maximum exposure length, as it is relatively easier to measure either using aerial imagery or laser rangefinder. Thus, Free Span Ratio is defined as follows,

$$FSR = \frac{MAFSL}{L_{bfw}} \tag{5.3}$$

If FSR is $\leq$ 1.0, the maximum exposure length or bankfull width of the river is more than the MAFSL, and hence the water crossing pipeline is said to be more vulnerable to VIV if it becomes exposed. On the contrary, if FSR exceeds 1.0, the pipeline is unlikely to fail due to VIV even if it becomes fully exposed as MAFSL is greater than the entire bankfull width of the river. Hence, we can find that the vulnerability of pipeline to VIV failure is inversely proportional to FSR.

5.6.1 Estimation of river bankfull width

Moody and Troutman developed power law relationships between river width (w), depth (d) and discharge (Q) based on data from a number of studies of world rivers that were used to characterize the two dimensional structure of channel networks [29]. The proposed relationships were:

$$w = 7.2 \times Q^{0.5 \pm 0.02} \tag{5.4}$$

$$d = 0.27 \times Q^{0.3 \pm 0.01} \tag{5.5}$$

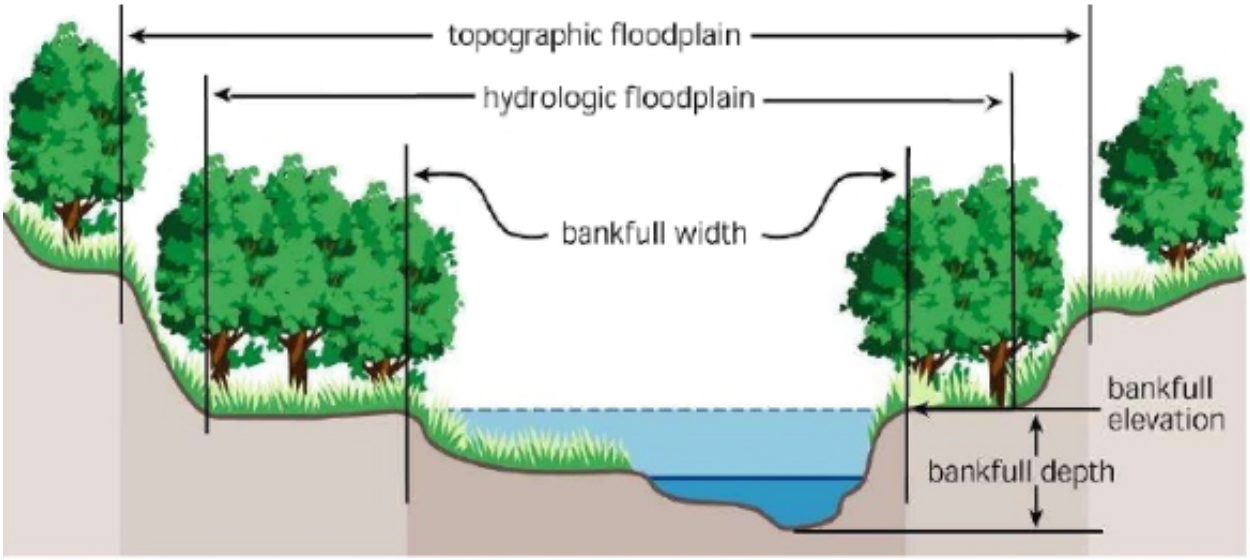

Figure 5.5: Stream Corridor Structure.
Note. Reprinted from [5]

Having predicted the MAFSL for all the 180 cases using ANN model, we can proceed to determine the vulnerability of these pipelines. Three values of the exponent namely 0.48, 0.5 and 0.52 are chosen to calculate the bankfull width using equation 5.4. Using the predicted MAFSL values and the bankfull width, the Free Span Ratio (FSR) is calculated for the entire data set. The calculated FSR values were found to be greater than 1 only for 4 out of the 180 cases when using all three values for the exponent value of discharge rate. In all the remaining cases, FSR was less than 1 indicating potential threat to flood induced VIV and further validates the real time data subject to failure of pipelines. This method of evaluating bankfull width and FSR can be considered as a preliminary screening tool to assess the situation. The vulnerability estimate could be refined by replacing the bankfull width with a more accurate or realistic value for the maximum exposure length.

6. CONCLUSION AND FUTURE WORK

Artificial Neural Network has helped develop a robust nonlinear model to predict critical span length and scour depth of river crossing pipelines. The focus is to determine suitable input features for the model. The overall influence of every input variable on the prediction model was analyzed in terms of its connection weights and their relative importance was ranked for each output. It is seen that factors such as Internal fluid pressure, dynamic lateral and vertical soil stiffness and age of pipeline have a significant contribution in terms of weights in the ANN model and hence, cannot be neglected. Best validation performance was observed at 11^{th} iteration, with a mean squared error value of 0.0129. Performance of training dataset reached its target mean squared error value of 0.001 after the 18^{th} iteration. More than 80% of the predicted values in the validation and testing dataset had less than 0.5% error. Free span ratio was calculated for all the cases and pipeline failure vulnerability was estimated as the inverse of Free Span Ratio. About 97.8% of the cases were found to be vulnerable to VIV failure which validates the model data.

This work can be further extended by collecting datasets for a particular pipeline or a specific river having large number of water crossing pipelines, leading to the development of prediction models for each pipeline and river. This way, all the unique environmental factors associated with each river and pipeline can be successfully captured. Emerging wireless solutions and sensor technologies enable unprecedented asset visibility and help understand pipeline behaviors under different conditions including structural loads, deflection, weather changes, soil characteristics, moisture and pH levels. This real time data from IoT based sensors play an important role to develop reliable prediction models and optimize the effective service life of a pipeline.

REFERENCES

[1] A. H. Haghiabi, "Prediction of River Pipeline Scour Depth using Multivariate Adaptive Regression Splines," *Journal of Pipeline Systems Engineering and Practice*, vol. 8, July 2016.

[2] J. Lee, *Introduction to Offshore Pipelines and Risers*. 2007.

[3] B. Guo, S. Song, A. Ghalambor, and T. R. Lin, "Chapter 5 - Pipeline Span," in *Offshore Pipelines*, pp. 53 – 63, Gulf Professional Publishing, Second Edition ed., 2014.

[4] J. T. V. Å$\frac{1}{2}$eljko Ivezic, Andrew J Connolly and A. Gray, *Statistics, Data Mining, and Machine Learning in Astronomy*. 2019.

[5] "Stream corridor restoration: Principles, processes and practices," *Federal Interagency Stream Restoration Working Group*, 1998.

[6] M. K. J. Julian D Olden and R. G. Death, "An accurate comparison of methods for quantifying variable importance in artificial neural networks using simulated data," *Ecological Modelling*, vol. 178, pp. 389–397, March 2004.

[7] "DNV Recommended Practice DNV-RP-F105 - Free Spanning Pipelines," February 2006.

[8] J. Olden and D. Jackson, "Illuminating the "black box": A randomization approach for understanding variable contributions in artificial neural networks," *Ecological Modelling*, vol. 154, pp. 135–150, 08 2002.

[9] C. Belvederesi, M. Thompson, and P. Komers, "Statistical Analysis of Environmental Consequences of Hazardous Liquid Pipeline Accidents," *Heliyon*, vol. 4, November 2018.

[10] G. Ferris, S. Newton, M. Ho, G. Eichhorn, and D. Bear, "Flood Monitoring for Buried Pipeline Watercourse Crossing," September 2015.

[11] H. O. Heggen, R. Fletcher, G. Ferris, and M. Ho, "Fatigue of Pipelines Subjected to Vortex-Induced Vibrations at River Crossings," September 2014.

[12] J. Xu, G. Li, J. Horrillo, Y. Rongmin, and L. Cao, "Calculation of Maximum Allowable Free Span Length and Safety Assessment of the DF1-1 Submarine Pipeline," *Journal of Ocean University of China*, vol. 9, March 2010.

[13] K. Koushan, "Vortex induced vibrations of free span pipelines," October 2019.

[14] L. Matta and R. Dotson, "Key considerations in the assessment of pipeline spans," *Pipeline Pigging Integrity Management Conference*, February 2015.

[15] M. Yaghoobi, S. Mazaheri, Said, E. Jabbari, and Ebrahim, "Determining Natural Frequency of Free Spanning Offshore Pipelines by Considering the Seabed Soil Characteristics," *Persian Gulf*, September 2012.

[16] O. Fyrileiv, K. MÃ¸rk, and K. Ronold, "Free Span Design according to the DNV-RP-F105 for Free Spanning Pipelines," January 2002.

[17] R. Barati, "Discussion of "Prediction of River Pipeline Scour Depth using Multivariate Adaptive Regression Splines by Amir Hamzeh Haghiabi," *Journal of Pipeline Systems Engineering and Practice*, May 2019.

[18] Y.-H. CHEN, J.-N. LI, K. LIAN, Q.-J. ZHU, and Y.-L. LIU, "Failure Prediction of Underground Pipeline Based on Artificial Neural Network," *DEStech Transactions on Computer Science and Engineering*, November 2017.

[19] *Pipeline Exposure at River Crossings: Causes and Cures*, vol. Volume 1: Risk Assessment and Management; Emerging Issues and Innovative Projects; Operations and Maintenance; Corrosion and Integrity Management of *International Pipeline Conference*, June 1998.

[20] A. Moncada-M. and J. Aguirre-Pe, "Scour below pipeline in river crossings," *Journal of Hydraulic Engineering, 125*, pp. 953–958, 1999.

[21] MMS, "Analysis and assessment of unsupported subsea pipeline spans. Minerals Management Service, USA," pp. 1–42, December 1997.

[22] A. H. Mouselli, "Offshore pipeline design, analysis, and methods.," *PennWell Publishing Co.*, pp. 50–52, 1981.

[23] O. Fyrileiv and L. Collberg, "Influence of Pressure in Pipeline Design - Effective Axial Force," *24th International Conference on Offshore Mechanics and Arctic Engineering*, June 2005.

[24] A. C. Nogueira and D. S. Mckeehan, "Chapter 11 - Design and Construction of Offshore Pipelines," in *Handbook of Offshore Engineering* (S. K. CHAKRABARTI, ed.), pp. 891 – 937, London: Elsevier, 2005.

[25] V. Skorpil and J. Stastny, "Neural Networks and Back Propagation algorithm," September 2006.

[26] A. Ooyen and B. Nienhuis, "Improving the convergence of the back-propagation algorithm," *Neural Networks*, vol. 5, pp. 465–471, December 1992.

[27] H. P. Gavin, "The Levenberg-Marquardt algorithm for nonlinear least squares curve-fitting problems," *Department of Civil and Environmental Engineering, Duke University*, August 2019.

[28] C. Dooley, Z. Prestie, G. Ferris, M. Fitch, and H. Zhang, "Approaches for evaluating the vulnerability of pipelines at water crossings," *Proceedings of the Biennial International Pipeline Conference, IPC*, vol. 2, September 2014.

[29] J. A. Moody and B. M. Troutman, "Characterization of the spatial variability of channel morphology," *Earth Surface Processes and Landforms*, vol. 27, pp. 1251–1266, September 2002.

APPENDIX A

MATLAB SCRIPT FOR ANN DEPLOYMENT

```
% Solve an Input-Output Fitting problem with a Neural Network
% Script generated by Neural Fitting app
% This script assumes these variables are defined:
% x - input data.
% t - target data.

sheet_name = "Normalized values" ;
num = xlsread ('Database and calculations.xlsx', sheet_name) ;
x = num (1:180, 1:12)' ;
t = num (1:180, 13:15)' ;

% Choose a Training Function
% For a list of all training functions type: help nntrain
% 'trainlm' is usually fastest.
% 'trainbr' takes longer but may be better for challenging problems.
% 'trainscg' uses less memory. Suitable in low memory situations.

trainFcn = 'trainlm' ;          % Levenberg-Marquardt backpropagation.

% Create a Fitting Network
hiddenLayerSize = 30 ;
net = fitnet ( [hiddenLayerSize   hiddenLayerSize], trainFcn ) ;
```

```
% Choose Input and Output Pre/Post-Processing Functions
% For a list of all processing functions type: help nnprocess
net.input.processFcns = 'removeconstantrows', 'mapminmax' ;
net.output.processFcns = 'removeconstantrows', 'mapminmax' ;

% Setup Division of Data for Training, Validation, Testing
% For a list of all data division functions type: help nndivision
net.divideFcn = 'dividerand' ;          % Divide data randomly
net.divideMode = 'sample' ;             % Divide up every sample
net.divideParam.trainRatio = 75 / 100 ;
net.divideParam.valRatio = 10 / 100 ;
net.divideParam.testRatio = 15 / 100 ;

% Choose a Performance Function
% For a list of all performance functions type: help nnperformance
net.performFcn = 'mse' ;                % Mean Squared Error

% Choose Plot Functions
% For a list of all plot functions type: help nnplot
net.plotFcns = {'plotperform' , 'plottrainstate' , 'ploterrhist' , 'plotregression' , 'plotfit'} ;
net.trainParam.max_fail = 20 ;
net.trainParam.min_grad = 1e-7 ;
net.trainParam.show = 10 ;
net.trainParam.lr = 0.01 ;
net.trainParam.epochs = 1000 ;
net.trainParam.goal = 0.001 ;
```

% Train the Network

$[net, tr]$ = train (net, x, t) ;

% Test the Network

y = net (x) ;

e = gsubtract (t, y) ;

performance = perform (net, t, y)

% Recalculate Training, Validation and Test Performance

trainTargets = t .* tr.trainMask{1} ;

valTargets = t .* tr.valMask{1} ;

testTargets = t .* tr.testMask{1} ;

trainPerformance = perform (net, trainTargets, y)

valPerformance = perform (net, valTargets, y)

testPerformance = perform (net, testTargets, y)

% View the Network

view (net)

figure, plotperform (tr)

figure, plottrainstate (tr)

figure, ploterrhist (e)

figure, plotregression (t, y)

figure, plotfit (net, x, t)

APPENDIX B

ILLUSTRATION TO QUANTIFY RELATIVE IMPORTANCE OF INPUT VARIABLES

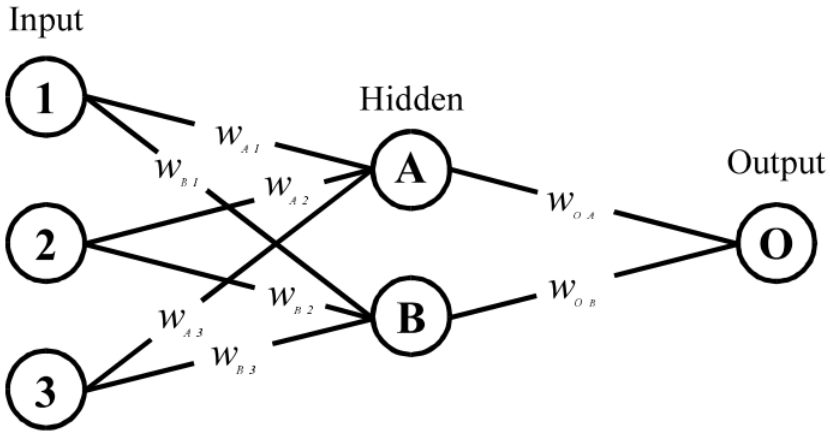

Figure B.1: Sample calculations shown for three input neurons (1, 2 and 3), two hidden neurons (A and B), and one output neuron (O). *Note.* Modified from [6]

Let us consider the model weights found after training the network to be as follows:

$\mathrm{W}_{A1} = -2.61$	$\mathrm{W}_{B1} = -1.23$
$\mathrm{W}_{A2} = 0.13$	$\mathrm{W}_{B2} = -0.91$
$\mathrm{W}_{A3} = -0.69$	$\mathrm{W}_{B3} = 2.09$
$\mathrm{W}_{OA} = 1.11$	$\mathrm{W}_{OB} = 0.39$

Table B.1: Input-hidden-output neuron connection weights

The overall connection weight which indicates the contribution of each input neuron to the output is calculated as follows:

Input 1	$(\mathrm{W}_{A1} \times W_{OA}) + (W_{B1} \times W_{OB})$	-3.37
Input 2	$(\mathrm{W}_{A2} \times W_{OA}) + (W_{B2} \times W_{OB})$	-0.21
Input 3	$(\mathrm{W}_{A3} \times W_{OA}) + (W_{B3} \times W_{OB})$	0.05

Table B.2: Overall connection weights corresponding to each input

The relative importance of an input variable is computed as a percentage of magnitude of its overall connection weight with respect to the summation of absolute values of overall connection weights of all input variables.

e.g., RI_1 = (3.37 / (3.37+0.21+0.05)) $\times 100 = 92.83\%$

	Relative Importance
Input 1	92.83 %
Input 2	5.8 %
Input 3	1.3 %

Table B.3: Relative Importance of input variables

APPENDIX C

TARGET AND PREDICTED VALUES OF THE DATASET

S.No	**Scour depth (in)**		**CSL for in-line motion (ft)**		**CSL for cross-flow motion (ft)**	
	Target	Prediction	Target	Prediction	Target	Prediction
1	12.073	12.072	9.410	9.409	15.262	15.262
2	11.487	11.491	12.351	12.352	20.020	20.018
3	10.208	10.191	17.302	17.297	28.691	28.692
4	9.694	9.707	19.397	19.400	32.381	32.378
5	6.210	6.209	30.694	30.695	52.868	52.870
6	6.211	6.211	30.745	30.745	52.958	52.957
7	6.212	6.212	30.770	30.769	53.003	52.999
8	6.215	6.216	30.791	30.790	53.040	53.042
9	5.435	5.443	9.925	9.929	16.237	16.234
10	5.435	5.439	9.938	9.939	16.259	16.258
11	5.436	5.436	9.946	9.945	16.273	16.274
12	5.442	5.434	9.948	9.945	16.277	16.279
13	6.681	6.690	115.271	116.115	194.906	196.308
14	6.681	6.683	116.222	116.223	196.514	196.514
15	6.681	6.679	116.250	116.249	196.562	196.563
16	6.681	6.675	116.410	116.286	196.832	196.627
17	9.832	9.836	7.583	7.584	12.868	12.869
18	9.834	9.835	7.587	7.585	12.874	12.872
19	9.838	9.834	7.588	7.588	12.877	12.878
20	9.841	9.832	7.593	7.589	12.884	12.881
21	4.612	4.612	15.310	15.304	23.715	23.710
22	4.612	4.611	15.321	15.328	23.732	23.744
23	4.613	4.614	15.325	15.319	23.739	23.727
24	4.613	4.613	15.329	15.332	23.745	23.748
25	12.132	12.151	20.268	20.279	32.538	32.549
26	12.142	12.146	20.274	20.275	32.547	32.546
27	12.147	12.143	20.287	20.285	32.569	32.570
28	12.154	12.139	20.297	20.291	32.585	32.586
29	12.814	12.811	94.881	94.879	167.740	167.741
30	12.817	12.834	94.987	94.982	167.934	167.909

S.No	Scour depth (in)		CSL for in-line motion (ft)		CSL for cross-flow motion (ft)	
	Target	Prediction	Target	Prediction	Target	Prediction
31	12.810	12.825	95.641	95.648	169.130	169.128
32	12.795	12.783	96.788	96.783	171.224	171.226
33	12.331	12.333	45.761	45.765	82.291	82.289
34	12.332	12.332	45.771	45.770	82.310	82.310
35	12.333	12.332	45.776	45.770	82.319	82.319
36	12.334	12.332	45.779	45.772	82.325	82.326
37	6.065	6.069	17.412	17.413	30.028	30.029
38	6.071	6.072	17.423	17.423	30.049	30.049
39	6.079	6.076	17.429	17.427	30.060	30.060
40	6.077	6.076	17.487	17.487	30.164	30.165
41	13.212	13.211	25.797	25.804	42.305	42.317
42	13.206	13.207	25.900	25.891	42.474	42.458
43	13.189	13.202	26.019	26.011	42.670	42.663
44	13.196	13.196	26.141	26.144	42.873	42.878
45	32.986	32.958	17.835	17.905	28.221	28.193
46	33.014	33.014	17.846	17.845	28.238	28.237
47	33.017	33.038	17.864	17.833	28.267	28.287
48	33.032	33.076	17.878	17.801	28.289	28.338
49	11.003	11.009	7.055	7.057	12.056	12.056
50	11.003	11.005	7.062	7.062	12.061	12.060
51	11.005	11.000	7.067	7.066	12.064	12.065
52	11.001	10.998	7.079	7.076	12.073	12.072
53	7.694	7.690	10.079	10.080	17.034	17.036
54	7.587	7.591	10.307	10.304	17.445	17.436
55	7.574	7.575	10.339	10.337	17.501	17.500
56	7.553	7.552	10.387	10.389	17.588	17.596
57	8.016	8.013	30.243	30.240	51.302	51.300
58	8.017	8.009	30.404	30.426	51.587	51.623
59	8.007	8.007	30.577	30.583	51.895	51.904
60	8.001	8.005	30.719	30.715	52.146	52.138
61	4.338	4.341	13.642	13.640	22.703	22.702
62	4.339	4.338	13.653	13.652	22.723	22.725
63	4.335	4.333	13.696	13.697	22.798	22.800
64	4.326	4.325	13.773	13.774	22.931	22.929
65	4.028	4.023	17.014	17.008	27.198	27.193
66	4.029	4.026	17.020	17.019	27.209	27.209
67	4.030	4.030	17.030	17.032	27.225	27.230
68	4.030	4.033	17.053	17.054	27.263	27.263
69	4.503	4.494	14.627	14.636	25.658	25.684
70	4.496	4.495	14.707	14.685	25.804	25.769

S.No	Scour depth (in)		CSL for in-line motion (ft)		CSL for cross-flow motion (ft)	
	Target	Prediction	Target	Prediction	Target	Prediction
71	4.496	4.499	14.734	14.736	25.853	25.854
72	4.495	4.502	14.765	14.774	25.909	25.917
73	9.236	9.238	14.848	14.845	24.041	24.043
74	9.236	9.237	14.850	14.850	24.045	24.046
75	9.237	9.236	14.852	14.853	24.048	24.046
76	9.237	9.236	14.853	14.855	24.050	24.047
77	4.474	4.469	72.113	72.112	124.082	124.080
78	4.474	4.471	72.174	72.149	124.187	124.145
79	4.474	4.474	72.195	72.206	124.223	124.242
80	4.474	4.475	72.232	72.221	124.288	124.268
81	32.709	32.710	36.895	36.896	114.608	114.609
82	32.726	32.724	36.896	36.895	114.605	114.606
83	32.733	32.732	36.898	36.900	114.596	114.599
84	32.737	32.738	36.902	36.903	114.583	114.583
85	29.438	29.439	35.077	35.076	97.088	97.089
86	29.453	29.452	35.078	35.078	97.086	97.086
87	29.459	29.459	35.080	35.081	97.080	97.080
88	29.463	29.463	35.084	35.083	97.071	97.071
89	16.355	16.354	21.476	21.475	40.226	40.225
90	16.363	16.363	21.476	21.477	40.226	40.226
91	16.366	16.367	21.478	21.477	40.227	40.227
92	16.368	16.369	21.480	21.478	40.229	40.230
93	14.203	14.205	39.544	39.545	66.475	66.475
94	14.202	14.204	39.577	39.607	66.534	66.591
95	14.207	14.206	39.598	39.598	66.571	66.572
96	14.209	14.207	39.624	39.622	66.617	66.618
97	13.257	13.257	44.225	44.218	76.943	76.938
98	13.251	13.247	44.404	44.410	77.274	77.279
99	13.237	13.232	44.693	44.709	77.810	77.824
100	13.210	13.220	44.997	44.985	78.372	78.363
101	5.105	5.105	25.805	25.800	43.457	43.448
102	5.105	5.105	25.837	25.844	43.514	43.525
103	5.102	5.103	25.929	25.912	43.673	43.643
104	5.102	5.102	25.952	25.950	43.713	43.710
105	10.557	10.555	12.659	12.644	20.440	20.396
106	10.558	10.550	12.669	12.673	20.455	20.453
107	10.550	10.544	12.695	12.707	20.495	20.518
108	10.531	10.539	12.734	12.730	20.558	20.560
109	3.458	3.452	50.447	50.448	97.659	97.673
110	3.458	3.455	50.524	50.521	97.809	97.809

S.No	Scour depth (in)		CSL for in-line motion (ft)		CSL for cross-flow motion (ft)	
	Target	Prediction	Target	Prediction	Target	Prediction
111	3.458	3.461	50.630	50.632	98.013	98.012
112	3.458	3.464	50.682	50.706	98.115	98.149
113	14.854	14.855	21.265	21.265	42.732	42.732
114	14.871	14.865	21.297	21.297	42.795	42.796
115	14.890	14.874	21.307	21.305	42.817	42.813
116	14.850	14.871	21.400	21.403	43.008	43.011
117	5.539	5.539	9.215	9.214	17.410	17.409
118	5.538	5.540	9.219	9.220	17.417	17.419
119	5.540	5.540	9.222	9.222	17.424	17.424
120	5.542	5.541	9.228	9.228	17.435	17.435
121	15.230	15.229	9.218	9.361	21.035	21.270
122	15.191	15.192	9.280	9.279	21.042	21.042
123	15.168	15.167	9.314	9.287	21.047	21.017
124	15.165	15.165	9.330	9.330	21.050	21.050
125	8.143	8.169	6.320	6.303	11.722	11.706
126	8.140	8.141	6.335	6.330	11.748	11.748
127	8.127	8.121	6.358	6.361	11.790	11.797
128	8.096	8.101	6.405	6.407	11.877	11.873
129	10.532	10.521	13.450	13.433	26.546	26.514
130	10.527	10.525	13.463	13.461	26.571	26.573
131	10.530	10.532	13.469	13.471	26.583	26.582
132	10.530	10.535	13.473	13.479	26.590	26.592
133	8.034	8.040	16.738	16.738	32.264	32.264
134	8.035	8.037	16.747	16.748	32.282	32.283
135	8.032	8.032	16.771	16.766	32.331	32.326
136	8.034	8.026	16.784	16.783	32.358	32.357
137	22.058	22.061	26.887	26.888	58.309	58.309
138	22.042	22.039	26.957	26.956	58.385	58.375
139	22.002	21.999	27.067	27.066	58.507	58.506
140	21.907	21.924	27.264	27.272	58.733	58.805
141	6.526	6.526	25.691	25.691	47.439	47.440
142	6.524	6.525	25.743	25.743	47.540	47.538
143	6.526	6.526	25.770	25.769	47.592	47.595
144	6.523	6.523	25.839	25.839	47.725	47.725
145	11.044	11.044	14.997	14.998	29.598	29.599
146	11.031	11.034	15.033	14.971	29.671	29.552
147	11.017	11.023	15.075	14.938	29.756	29.495
148	10.985	11.014	15.151	14.888	29.912	29.424
149	12.633	12.631	13.478	13.476	24.436	24.437
150	12.629	12.632	13.492	13.493	24.452	24.451

S.No	Scour depth (in)		CSL for in-line motion (ft)		CSL for cross-flow motion (ft)	
	Target	Prediction	Target	Prediction	Target	Prediction
151	12.610	12.610	13.528	13.529	24.491	24.492
152	12.587	12.585	13.571	13.570	24.539	24.539
153	27.316	27.341	29.072	29.067	61.309	61.299
154	27.139	27.107	29.414	29.420	61.869	61.882
155	26.915	26.859	29.813	29.834	62.541	62.589
156	26.395	26.404	30.725	30.723	64.137	64.133
157	17.942	17.930	48.625	48.640	95.395	95.461
158	17.941	17.940	48.654	48.653	95.454	95.453
159	17.938	17.947	48.684	48.682	95.515	95.484
160	17.937	17.960	48.718	48.696	95.585	95.473
161	9.045	9.044	14.541	14.541	26.142	26.143
162	9.045	9.046	14.545	14.545	26.151	26.152
163	9.041	9.046	14.559	14.634	26.176	26.294
164	9.039	9.046	14.567	14.689	26.190	26.382
165	3.041	3.034	10.447	10.472	18.237	18.243
166	3.041	3.037	10.450	10.464	18.243	18.243
167	3.041	3.040	10.457	10.459	18.254	18.251
168	3.040	3.042	10.469	10.466	18.276	18.279
169	9.813	9.813	14.574	14.576	27.103	27.104
170	9.818	9.818	14.575	14.574	27.103	27.103
171	9.820	9.820	14.576	14.575	27.105	27.106
172	9.821	9.820	14.577	14.577	27.108	27.110
173	17.922	17.924	24.588	24.585	52.407	52.409
174	17.922	17.920	24.596	24.600	52.417	52.415
175	17.915	17.915	24.619	24.620	52.445	52.444
176	17.910	17.912	24.632	24.630	52.460	52.461
177	3.892	3.895	3.451	3.449	5.984	5.987
178	3.893	3.892	3.452	3.451	5.986	5.985
179	3.889	3.888	3.458	3.459	5.997	5.997
180	3.886	3.884	3.464	3.467	6.008	6.007